



**Restricted document**

***Saline Aquifer CO<sub>2</sub> Storage (SACS)  
Feasibility study of microseismic monitoring  
(Task 5.8)***

Research carried out in the framework of the EU project n° ENK6-CT-1999-00014  
"SACS2"

H. Fabriol

December 2001  
BRGM/RP-51293-FR



Key words: Carbon dioxide, storage, microseismicity, monitoring

The reference citation for this report is as follows:

Fabriol H. (2001) - Saline Aquifer CO<sub>2</sub> Storage (SACS), Feasibility study of microseismic monitoring (Task 5.8). BRGM/RP-51293-FR, 23 Fig, 3 Tabl.

© BRGM, 2001 this document is not to be reproduced, in part or in whole, without the express permission of the BRGM.

## Synthesis

This report evaluates the practicality and advantages of microseismic monitoring as a tool for detecting the distribution of CO<sub>2</sub> in a storage reservoir. Chapter 1 reviews microseismic monitoring using examples taken from published papers on gas storage and fluid injection in mainly sedimentary reservoirs. Chapter 2 covers downhole instrumentation as well as data processing and interpretation. Chapter 3 addresses the real possibility of using microseismic monitoring at Sleipner based on the reference list and studies of the state of stress in the North Sea. Chapter 4 concludes with proposals for the installation of one or more permanent sensors for microseismic monitoring in a future observation well.

We begin by recognizing that numerous mechanisms generate induced microseismicity: gas storage, EOR (enhanced oil recovery) using CO<sub>2</sub> or hydraulic fracturing, fluid injection, production-related reservoir compaction, etc. Although the low porosity of carbonates and sandstones is a contributing factor in the occurrence of hundreds of microearthquakes, examples of high-porosity environments (Lower Frio and Ekofisk) show that this is not the only trigger. However, the first example involves the injection of fluids into sandstone and the second, production-related compaction. The number of events recorded is relativized by the distance between the source and the measuring device.

Because of the magnitude of microearthquakes, borehole sensors must be used within a few hundred metres of the sources. Tools with 12, 24 or 48 x three-component sensors are now in common use for semi-permanent observations of a few months' duration. Permanent sensors placed between the tubing and the casing or cemented behind the casing can be used for a permanent network. Methods of processing large masses of data have greatly improved and software is readily available for purchase.

In light of the porosity values (about 27%) at Sleipner, microearthquakes are unlikely to occur in the Utsira Formation, except in shale lenses or at the top of the formation. This latter case could be the most interesting, as it would indicate the presence of leakage in the caprock. Given these conditions, microseismic monitoring would not be the preferred tool for monitoring CO<sub>2</sub> injection. However, in terms of drilling observation wells, we recommend:

- choosing the option of installing permanent geophones on the tubing of well 2 for repeated VSP;
- adding a system for continuously recording seismic background noise using these sensors.

With this, it would be possible to detect any microearthquake that is located within approximately one kilometre of the well and to attempt to associate it with the shales of the Utsira Formation or those of the overlying Nordland Formation. The additional cost of a permanent recording system and one year of data processing is estimated at about 92,000 €.

Even if microseismicity monitoring has not proven to be very suitable at Sleipner, the examples reviewed in chapter 2 show that it could be appropriated to other CO<sub>2</sub> underground storage projects, particularly in low permeability reservoirs. Consequently, we suggest including it in the SACS "Best Practise Manual" for CO<sub>2</sub> storage in saline aquifers.

## Contents

<b>Introduction .....</b>	<b>7</b>
<b>1. Microseismic monitoring: a review.....</b>	<b>11</b>
1.1 Microseismicity induced by underground gas storage (Germigny-sous-Coulombs, France) .....	11
1.2 Microseismicity induced by fluid injection (Frio Formation, Beaumont solid waste storage site, Texas, USA) .....	15
1.3 Microseismicity induced by fluid injection (Cotton Valley gas field, Texas, USA) .....	17
1.4 The Ekofisk oil field experiment .....	23
1.5 Geothermal fields and hydraulic fracturing .....	23
1.6 Conclusions .....	24
<b>2. Data acquisition and processing.....</b>	<b>27</b>
2.1 General .....	27
2.2 Sensors and recording system .....	27
2.2.1 Wireline monitoring .....	27
2.2.2 Permanent monitoring .....	30
2.3 Location methods .....	32
2.4 Conclusions .....	35
<b>3. What could be expected at Sleipner.....</b>	<b>37</b>
3.1 Seismological data .....	37
3.2 Downhole measurements.....	37
3.3 Origins of the present-day stress field in the North Sea.....	40
3.4 Conclusion.....	40
<b>4. Proposals for a field experiment .....</b>	<b>43</b>
<b>5. Conclusion .....</b>	<b>45</b>
<b>6. References .....</b>	<b>47</b>
<b>List of figures .....</b>	<b>51</b>

## List of appendices

Appendix 1: A brief insight into seismic hazard .....	55
Appendix 2: Magnitude proposal for follow up of the seismic network and design, setting and periodical update of the automatic monitoring procedures. .	61



## Introduction

### GREENHOUSE GAS REDUCTION AND CO<sub>2</sub> STORAGE

Most scientists and decision makers now agree that the accumulation of greenhouse gases is partly responsible for global warming. Carbon dioxide accounts for about two thirds of these gases. Limiting CO<sub>2</sub> emissions will therefore be crucial over the next few decades and constitutes part of the resolutions adopted at the 1992 Earth Summit held in Rio de Janeiro.

Several options are available for reducing emissions: increasing energy efficiency or using forms of energy such as nuclear or renewable energy that do not emit CO<sub>2</sub> (Herzog *et al.*, 2000). However, sequestering represents a third possibility that, if managed correctly, could get us through the next few decades before forms of “clean” energy, or energy that does not emit greenhouse gases or produce hazardous waste, are brought on stream.

The first type of storage is natural storage in plants, soil or forests, i.e. the well known carbon “sinks” that offer the advantage of sequestering the CO<sub>2</sub> that exists in the air without the need for sophisticated installations, which can be very useful near or within built-up areas. Storage strategies will necessarily involve forest planting or reforestation.

Underground or undersea storage is an alternative that has aroused considerable interest over the past few years. Its principle is simple: collect CO<sub>2</sub> emitted on a huge scale by chemical factories or thermal power plants and inject it into the sea or the subsurface.

Oceans represent the largest existing potential reservoir for the storage of anthropogenic carbon dioxide. If an amount of CO<sub>2</sub> equal to that emitted since the middle of the nineteenth century were to be reinjected into the ocean, it would add only 2% to the total amount of dissolved CO<sub>2</sub> that already exists in the oceans. Injection can be done in many ways, for example by using conduits either to below 1000 m so that CO<sub>2</sub> will dissolve in sea water, or to below 3000 m to form lakes of CO<sub>2</sub> that would remain stable for several hundred years.

Although for now the storage of CO<sub>2</sub> in oceans is still the subject of scientific research, underground storage has given rise to several pilot projects, including the Sleipner project already underway in Norway. Indeed, CO<sub>2</sub> injection into oil reservoirs has been used for several decades to increase the mobility of oil and facilitate its recovery (EOR, or enhanced oil recovery).

### THE INDUSTRIAL OPERATION AT SLEIPNER AND THE ASSOCIATE EUROPEAN RESEARCH PROJECT

Sleipner is a producing oil and natural gas field in the North Sea. It lies within Norwegian territorial waters, about halfway between Aberdeen and Bergen (Fig. 1).

Since 1996, carbon dioxide associated with the natural gas extracted by Statoil from one of the producing reservoirs at over 2500 m depth, has been reinjected at 1000 m into the sandy Utsira Formation (Fig. 2). About one million of metric tons are reinjected per year. For a country such as Norway, this represents about 3% of the total amount of CO<sub>2</sub> emitted and, because of the high taxes on CO<sub>2</sub> offshore emissions, the cost of the reinjection well and installations were amortized in under two years.



**Fig. 1:** Location of the Sleipner hydrocarbon field

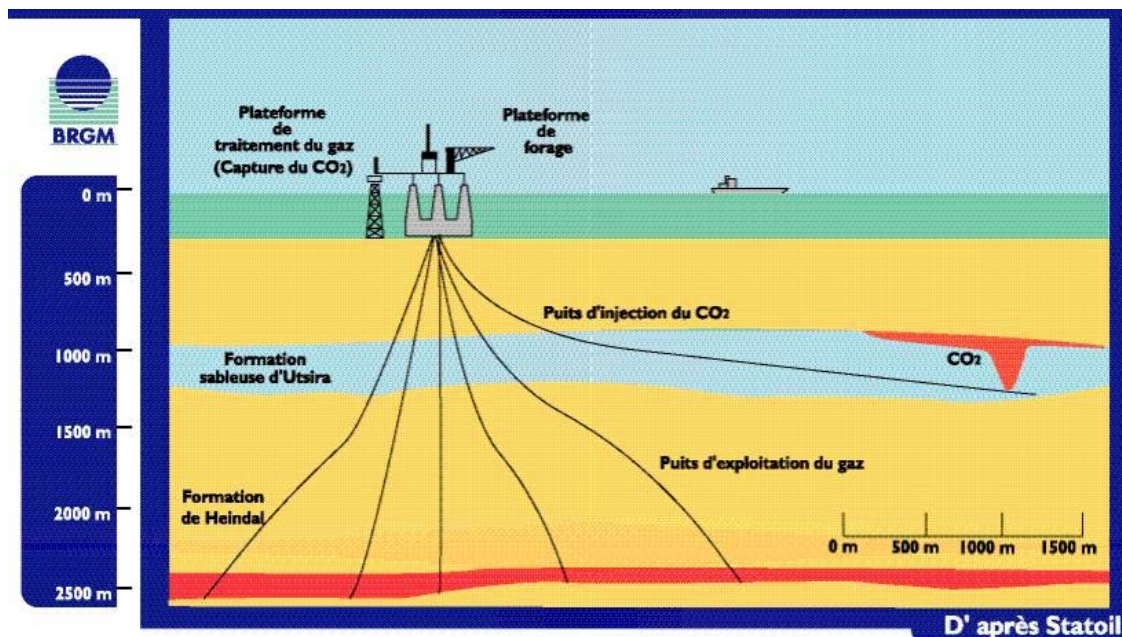


**Fig. 2:** Principle of CO<sub>2</sub> sequestering at Sleipner.

Detailed preliminary studies were carried out to ensure the technical and economic feasibility and the safety of the Sleipner project. Subsequently, a consortium of oil companies and public scientific institutions found it necessary to delve further into the physico-chemical behaviour of the stored CO<sub>2</sub> and its migration in the Utsira Formation. This is the objective of the European project “ Saline Aquifer CO<sub>2</sub> Storage ” (SACS2), of which this study is part (Thermie project SACS, Phase 1, from november 1998 to december 1999 – contract OG/306/98/NO, followed by the Energy project SACS2, Phase 2, from avril 2000 to march 2002 – contract ENK6-CT-1999-00014).

4-D seismic reflection (or time-lapse seismics) is the geophysical method that provides us with the most accurate true position of the so-called bubble of injected CO<sub>2</sub>. It involves using seismic profiles established at regular intervals over time to compare changes in reflectivity (of seismic reflectors) due to the presence of CO<sub>2</sub>. A comparison between seismic reflection work carried out in 1994 and in September 1999 highlights the presence of CO<sub>2</sub> bubbles visible on Fig. 3. The CO<sub>2</sub> is currently concentrated under thin sandstone layers and is migrating upward by buoyancy and upward from layer to layer through zones of higher porosity. The CO<sub>2</sub> is likely to be more diffuse from one layer to another.



**Fig. 3:** *Interpretation of the comparison between seismic work from 1994 and 1999. The iso-surfaces correspond to a factor 3 increase in reflectivity compared to the original top Utsira reflection. The green surface is top Utsira and the blue surface is base Utsira (SACS2 internal report, 2000).*

Microseismic monitoring is a passive seismic technique that has been proposed to accompany 4D seismics, which uses an artificial source. Although microseismic monitoring does not have the spatial resolution of 4D seismics, it can be used to detect, within a few tens of metres or even a few metres, zones in which local stress

accumulation could cause sudden failure and therefore a microearthquake. Moreover, microseismicity monitoring has the advantage to be continuous. The objectives of this report are to examine whether or not microseismic monitoring would be useful in the case of CO<sub>2</sub> storage at Sleipner and to improve our understanding of how migration occurs.

## **INDUCED MICROSEISMICITY - GENERAL**

Induced microseismicity is a well known phenomenon that can be detected in mines (also known as microseismic or seismo-acoustic emission), during and after dam impoundment (also known as reservoir-induced seismicity), or as a consequence of fluid injection at depth (also known as acoustic emission).

Microseismic events in mines are mainly due to deformation and cracking of the rock body around an opening, as a result of stress redistribution. Monitoring of these microseismic events is widely used for rockburst prediction (Srinivasan *et al.*, 1999).

Fluid injection can also induce seismicity. Reservoir-induced seismicity is commonly observed during the first filling of a reservoir or following rapid changes in water level (Simpson *et al.*, 1988). The magnitude of such earthquakes can be as high as 5.5 and 6.3, for the two Koyna earthquakes in India (1967). The second earthquake killed 200 people and injured over 1500. It is now accepted that two mechanisms are involved: first the loading of the reservoir for the earthquakes occurring shortly after the start of filling, and second the increase in pore pressure for the delayed seismicity, through the decrease in effective stress.

Finally, induced microseismicity is generated when fluid is injected into deep reservoirs for hydraulic fracturing experiments to increase permeability, for waste fluids storage, for EOR, etc. In this case the main factor is the increase in pore pressure and the corresponding decrease in effective pressure on weak joints or faults.

## **OBJECTIVES OF THIS STUDY**

This report evaluates the practicality and advantages of microseismic monitoring as a tool for detecting the distribution of CO<sub>2</sub> in a storage reservoir. The chapters are organized as follows: Chapter 1 reviews microseismic monitoring using examples from published papers on gas storage and fluid injection in mainly sedimentary reservoirs. Chapter 2 covers downhole instrumentation as well as data processing and interpretation. Chapter 3 addresses the real possibility of using microseismic monitoring at Sleipner based on the reference list and studies of the state of stress in the North Sea. Chapter 4 concludes with proposals for the installation of one or more permanent sensors for microseismic monitoring in a future observation well. Appendix 1 touches briefly on the problem of seismic hazards associated with the sequestering of CO<sub>2</sub> in the North Sea.

# 1. Microseismic monitoring: a review

This chapter reviews seismic monitoring using examples taken from the literature. References were selected in the following order:

- microseismicity induced by underground gas storage;
- microseismicity induced by fluid injection for underground waste storage or hydrocarbon production;
- Ekofisk;
- Hot Dry Rocks (HDR) geothermal projects.

The reference from which the information is taken is provided at the beginning of each example.

## 1.1 MICROSEISMICITY INDUCED BY UNDERGROUND GAS STORAGE (GERMIGNY-SOUS-COULOMBS, FRANCE)

Deflandre, J.P., Laurent, J., Michon, D. and Blondin, E., 1995, *Microseismic surveying and repeated VSPs for monitoring an underground gas storage reservoir using permanent geophones*, First Break, Vol. 13, No. 4, 129-138.

This example is one of the rare published cases of recorded microseismicity induced by the storage of natural gas in deep geological structures. It involves the site at Germigny-sous-Coulombs (Paris Basin, France) where natural gas is stored in the summer and withdrawn in the winter. The reservoir is an anticline located at a depth of 740 m below sea level (bsl) in Early Cretaceous sand layers interbedded between sandstone and shales (Fig. 4). Between 1983, when storage began, and 1993, the total volume injected was positive, i.e. the volume injected each summer was greater than that withdrawn the following winter. The boundaries of the gas bubble were deduced from well observations (Fig. 4); its surface area has increased and in particular migration has occurred beyond well MC7, which contains the geophone string.

Recordings were made in July and October 1991 and in April 1992. The measuring device comprised three x three-component geophones placed between the tubing ( $\varnothing 2 \frac{7}{8}$ " ) and the casing ( $\varnothing 7$ " ) at depths of 783, 815 and 905 m below ground level in observation well MC7 (Fig. 5). This well is normally used for measuring gas saturation by neutron logging. Geophones are clamped to the casing using two springs that are set into place remotely from the surface at the desired depth. Nine signals are sent to the surface in analogue form using a conventional seven-conductor cable. Sampling frequency is 4 kHz per channel. Seismic events are stored on disk providing that the acquisition criteria are met.

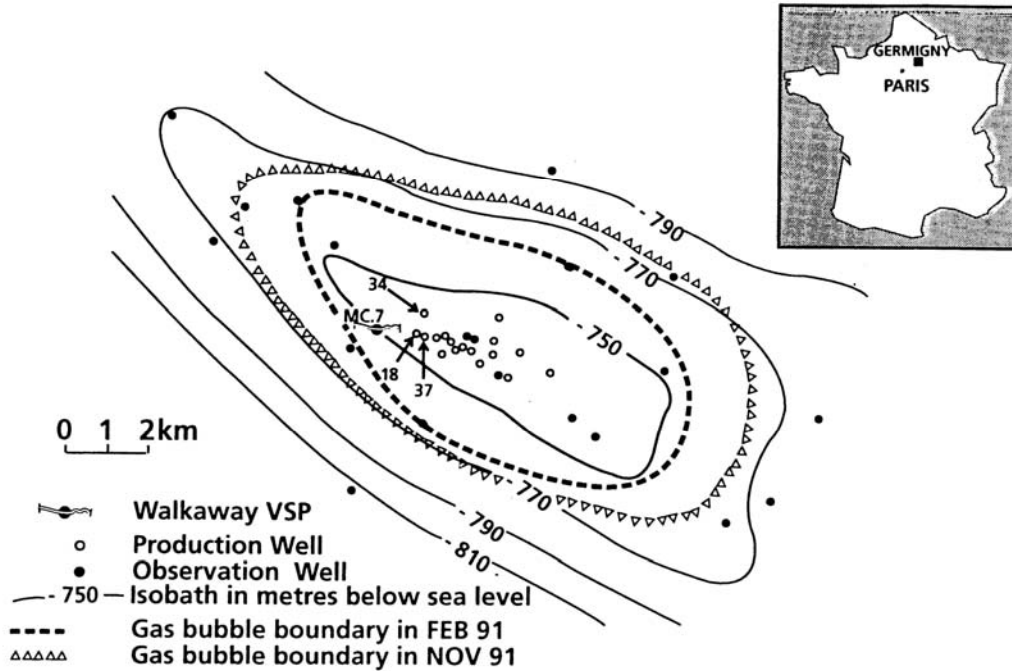


Fig. 4: Germigny-sous-Coulombs gas storage facility. Map of the isobaths of the Wealden reservoir top. Location of well MC7 and extent of the gas bubble in February and November 1991 are shown (from Deflandre et al., 1995).

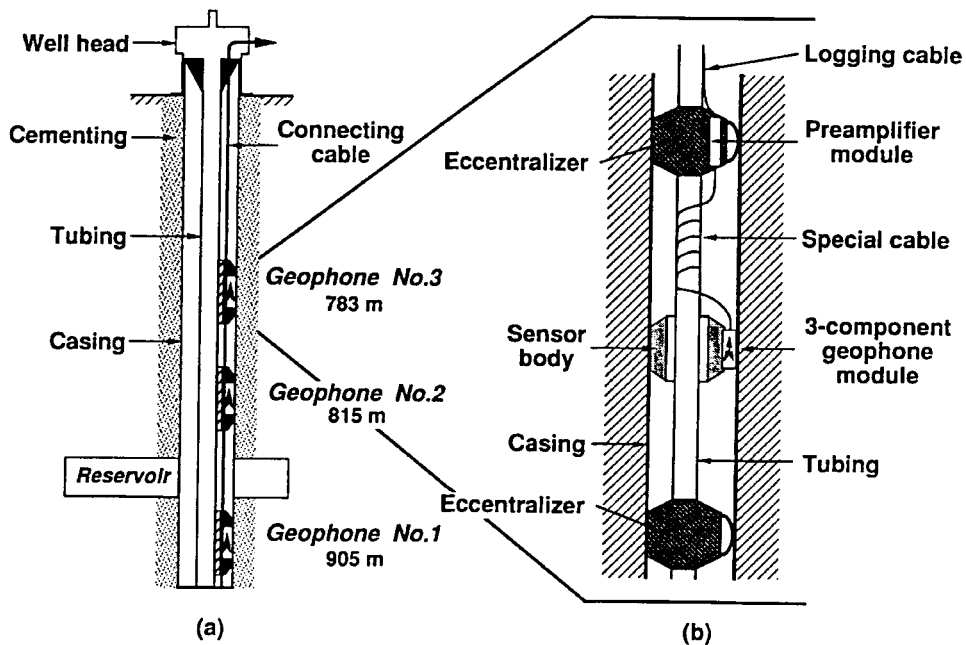
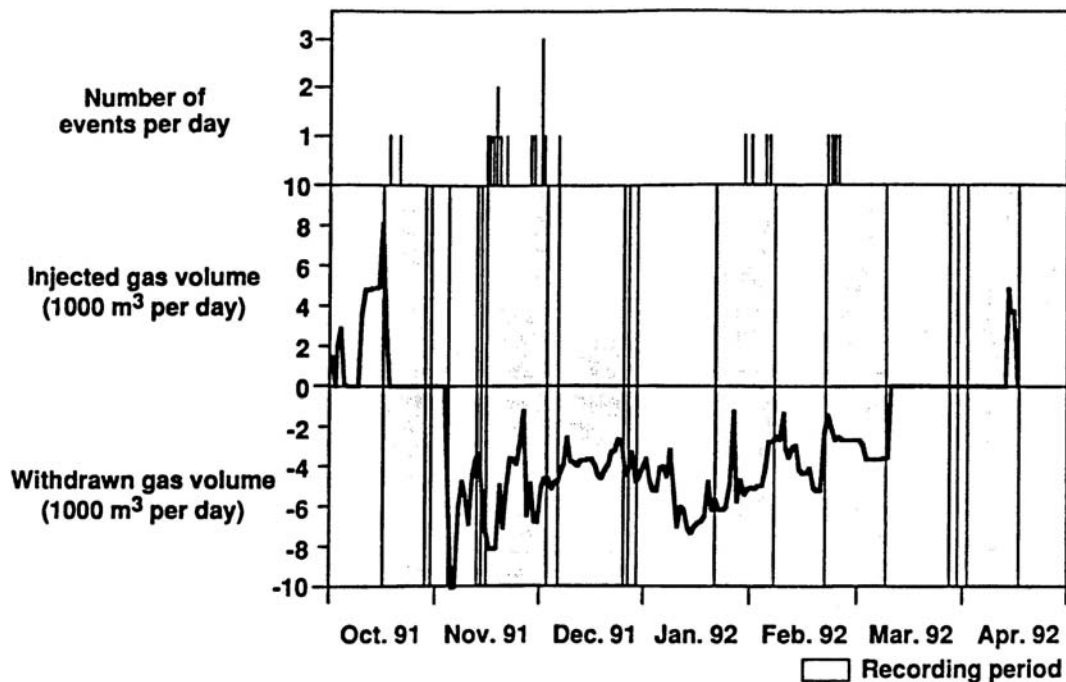


Fig. 5: On-tubing permanent geophones: a) schematic diagram of the three-level string inside well MC7; b) detailed diagram of an on-tubing permanent geophone (op. cit.)

Twenty-seven events were recorded during the three recording periods, with a maximum of three per day. They seem to be associated with variations in the volumes injected or withdrawn (Fig. 6) and not with periods of stability (constant flow rate or no injection or withdrawal). The absence of events in the April 1992 recording may also be due to a delay between the appearance of microseismicity and the advance of the injected gas.



**Fig. 6:** Relationship between acoustic activity and variations of gas volumes in relation to injection and withdrawal (over a seven-month period). The survey periods are shown by grey areas. Negative values correspond to gas volumes withdrawn and positive ones to injected volumes. The number of microseismic events recorded per day (one to three) is given in the histogram in the upper part of the figure (*op. cit.*).

Microearthquake foci were located by triangulation between receivers and, where possible, wave polarization analysis, i.e. when P- and S-wave arrivals were well differentiated. Fig. 7 shows the location of recorded events projected onto a plane passing through the axis of well MC7, azimuth information being more difficult to define. The diameter of the points is proportional to the magnitude, calculated from the duration of the microearthquake. This estimate provides values greater by at least one unit than the values obtained by calculating the moment magnitude from the amplitude spectrum.

Microearthquakes can be classified into two main groups:

- events located nears levels C1 and C5 (Fig. 7);
- events located above 800 m.

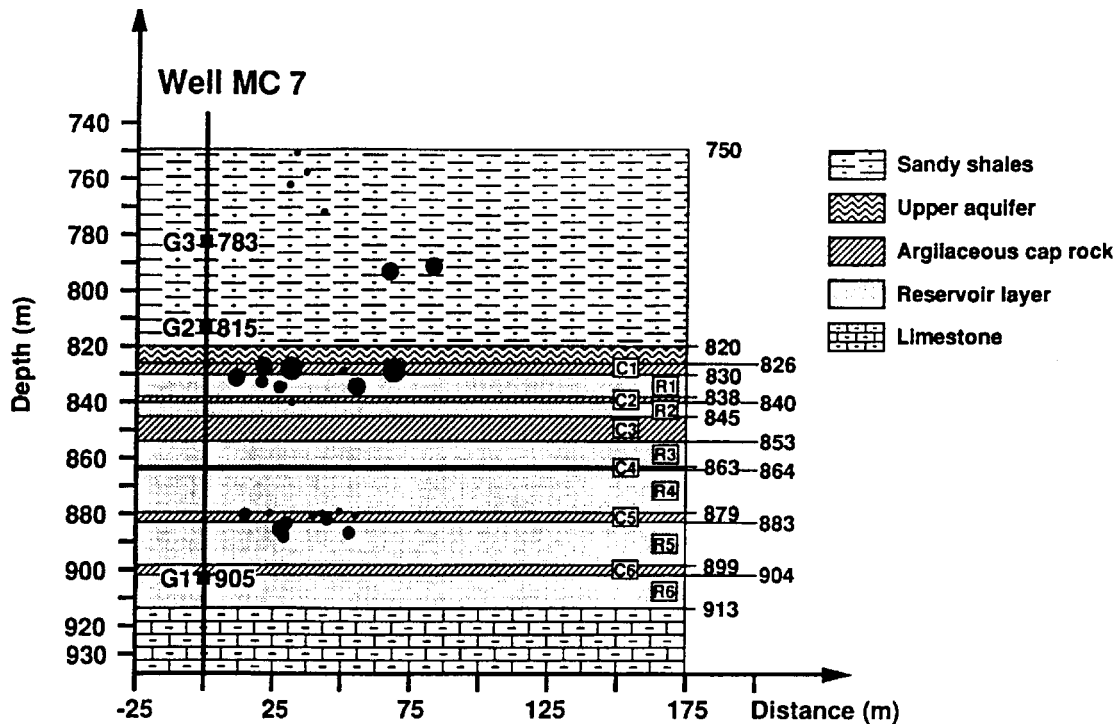


Fig. 7: 2D location of microseismic events. G1, G2 and G3 are sensors (op. cit.)

The authors suggest that the first group of events is located at the top and bottom of the gas-saturated layers (R1 and R3), as was confirmed through neutron logging, or hydraulically connected to these layers (R4). This microseismicity therefore defines the boundaries of the active part of the reservoir where gas can be stored. Group 2 events are located above the reservoir in sandy shale where the mean pressure increase is 0.04 MPa for pressure variations of 1.5 to 2.5 MPa in the reservoir. In fact, stress variations induce pore pressure variations in a large volume of the well-drained upper aquifer (porosity of 20% and permeability of 1D).

Events in both groups are induced by stress redistribution due to pore pressure variations in the reservoir caused by gas injection and withdrawal. For events in group 1, stress variations generate microseismicity at the boundaries of the layers where pore pressure changes, i.e. at the interface between permeable and impermeable layers. For events in group 2, as there is no hydraulic continuity between fluids in the upper aquifer and those in the reservoir, microseismic activity is triggered more by mechanical effects than by hydraulic effects. Variations in effective stress in these layers depend more on a change in the *in situ* state of stress than on pore pressure. Variations in pore pressure outside the reservoir may be due to matrix compressibility effects. Unfortunately, it was not possible to measure pore pressure around well MC7.

The microseismic monitoring experiment at Germigny-sous-Coulombs is the first of its kind to be carried out in a gas storage reservoir using permanent sensors placed between

tubing and casing. Results show that gas injection/withdrawal in a poorly fractured reservoir induces microseismicity and that location of the events allows an accurate identification of reservoir beds. However, the scope of the geophone investigation was limited to about 100 m from the observation well, because of the very low magnitude of the events.

## **1.2 MICROSEISMICITY INDUCED BY FLUID INJECTION (FRIO FORMATION, BEAUMONT SOLID WASTE STORAGE SITE, TEXAS, USA)**

Phillips, W.S., Rutledge, J.T., House, L.S. and Fehler, M.C., 2000, *Induced microearthquake patterns in hydrocarbon and geothermal reservoirs*, submitted to *Pure and Applied Geophysics*, March, 2000.

The object of the Frio experiment was to investigate the use of hydraulic fracturing for the underground storage of solid waste. A volume of 8000 m<sup>3</sup> of fluids and solids of unspecified nature was injected, in October 1993 at between 1349 m and 1407 m depth, into the highly permeable and unconsolidated Lower Frio sandstone near Beaumont in Texas. The Lower Frio Formation is underlain and overlain by impermeable shales.

Monitoring of induced microseismicity was carried out using two strings of 25 x three-component geophones cemented at 9-m intervals in two observation wells (Fig. 4 from Phillips *et al.*, 2000). Nearly 2900 seismic events were recorded during the entire experiment. Only 54 of these were located reliably, the magnitude of the others being too small. The 54 epicentres were located southwest of the injection well (Fig. 8), either immediately around the well or along a southwest alignment oriented radially with respect to the well. It is interesting to observe the development of such a well defined alignment, which is inconsistent with the unconsolidated nature of the Lower Frio Formation. The authors also observed a migration of events toward the injection well.

Microseismicity tends to become organized along thin horizontal strands of activity, which may be related to stratigraphic variations in mechanical properties, such as the increased ductility of a layer compared its enclosing layers or, in the case of these enclosing layers, increased mechanical strength and capacity to support stress.

An examination of spatial distribution evolution with time improves our understanding of the generation of microseismicity. If microseismicity were due to fracture extension, it should evolve away from the injection well. Such behaviour was observed at the Lower Frio, but only during the first stage of injection. Later, the opposite occurred: microseismic events occurred closer and closer to the injection well, as at Cotton Valley (see the next example).

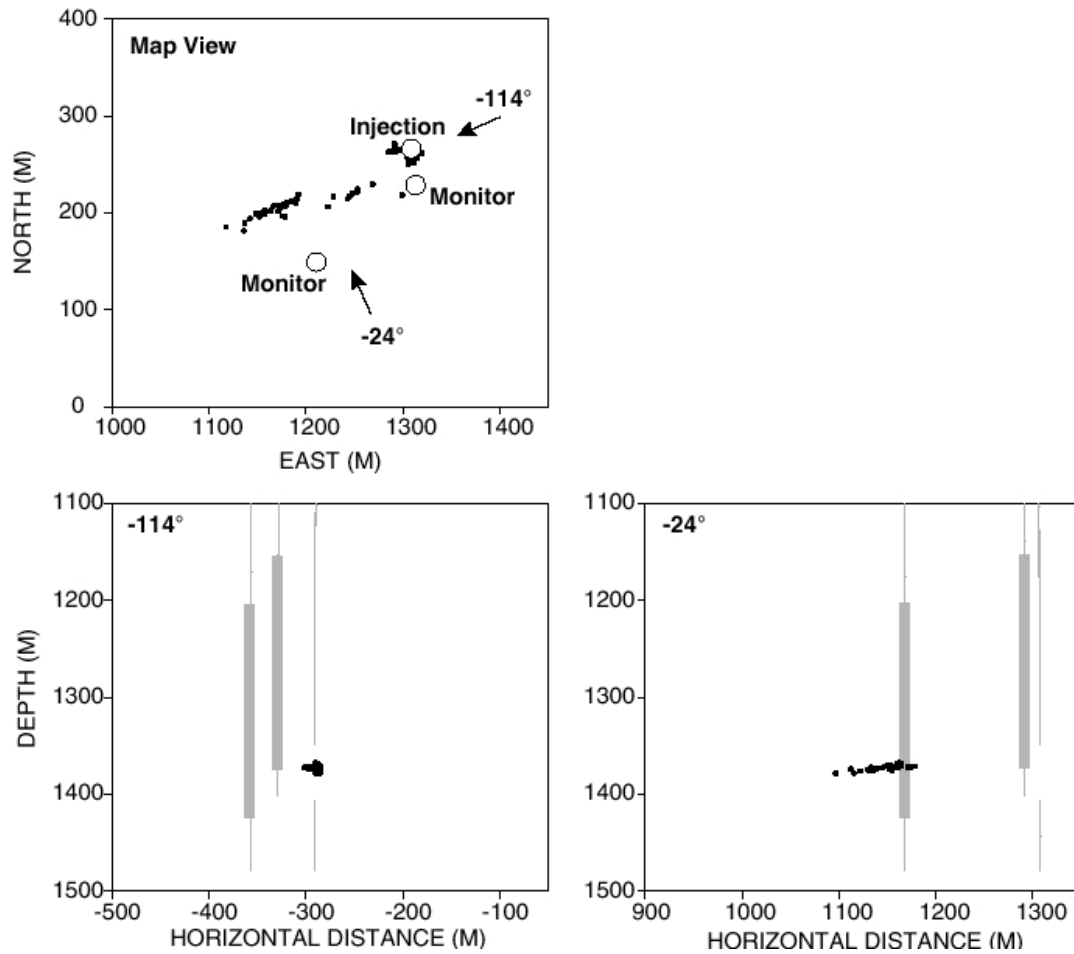


**Fig. 8:** *Map and cross-section views of events located in the Lower Frio during the waste injection experiment. Arrows show cross-section view directions. In cross section views, the thick lines represent the geophones string locations. The gap in the injection well represents the injection interval (from Phillips et al., 2000).*

The authors provide the following explanation. The inflating fracture is oriented normal to the minimum principal stress  $\sigma_3$  and supports little resolved shear. This makes it difficult to find the initial mechanical conditions to trigger slip. Withers and Rieven (1996) observed that at the Lower Frio, events increase in magnitude with increasing distance from the injection point during pressurization, because of an increase in stress at the fracture tip with time. Once slip is initiated at a point, local stresses are modified, which promotes slip at other points. If slip initiation occurs far from the injection point, microseismicity will migrate preferentially toward the injection point, because pore pressure is higher in that direction. Thus, the stress induced by initial slip is responsible for the reverse migration of microearthquakes.

### 1.3 MICROSEISMICITY INDUCED BY FLUID INJECTION (COTTON VALLEY GAS FIELD, TEXAS, USA)

Rutledge, J.T. and Phillips, W.S., 2001, *High-resolution microseismic imaging of a hydraulic fracture, Carthage Cotton Valley gas field, East Texas*, submitted to *Geophysics*, March 2001.

The case of the Cotton Valley gas field is interesting as it involves EOR by hydraulic fracturing with the injection of water and proppants in low-porosity (average 9.3%) sands interbedded between shales. This project, carried out in 1997, involved systematic microseismic monitoring and produced a data set that was exceptional in terms of quality, instrument coverage and variety in treatment design. Six stimulation operations were carried out at three different levels in two wells. The orientation, length and thickness of the stimulated zones were determined by locating microearthquake sources.

The stress state at Cotton Valley is characteristic of an extensional regime with normal faulting; the minimum horizontal stress ( $S_{hmin}$ ) is oriented north-northwest, as deduced from observations of recent tectonism in the zone, hydraulic fracture stress tests, borehole breakouts and coring-induced fracture orientations. Stimulation was therefore likely to a) create artificial fractures with the same orientation as the natural fractures, i.e. vertical striking east-northeast and parallel to  $S_{Hmax}$ , or b) affect pre-existing fractures with the same orientation.

The paper presents a detailed analysis of one of the six stimulation operations carried out at level 3 in injection well 21-10 (Fig. 9). Microseismicity monitoring was done in two observation wells using 715-m-long strings of 48 x three-component geophones. Sensors were permanently installed, i.e. attached to the production tubing and cemented into the wells. The treated section in stage 3 measured 80 m, with six perforated intervals over a cumulative height of 24 m.

Injection occurred in three phases: water, viscous gel with a sand proppant and finally water for flushing (total volume 1253 m<sup>3</sup>). Locations were determined for 696 of the 1122 microearthquakes recorded. Fig. 10 shows variations in the number of microearthquakes and pressure with time. As is usual in stimulation operations based on hydraulic fracturing, microseismicity increases with increasing pressure, with an additional significant effect from the injection of sand.

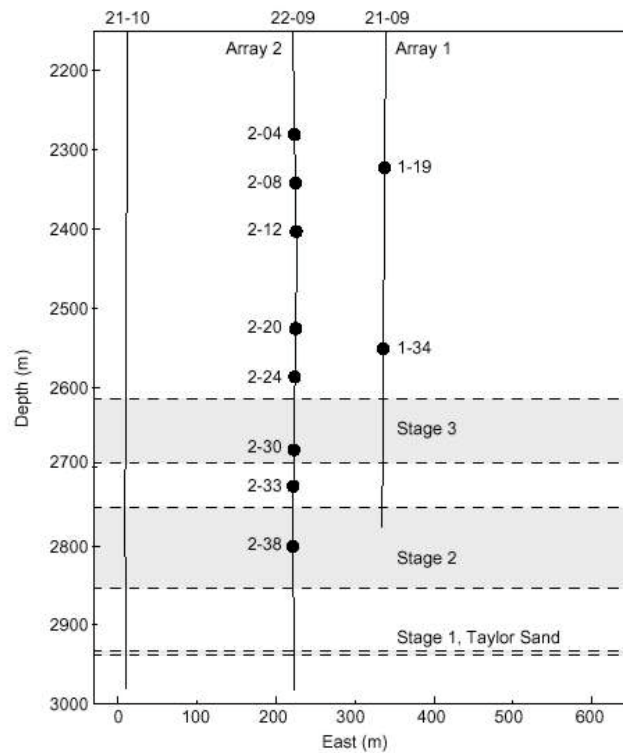


**Fig. 9:** Depth view of treatment and monitor wells. Three hydraulic fracture completion stages were conducted in the treatment well 21-10. Geophone stations used in determining the stage 3 microearthquake locations are shown (from Rutledge and Phillips, 2001).

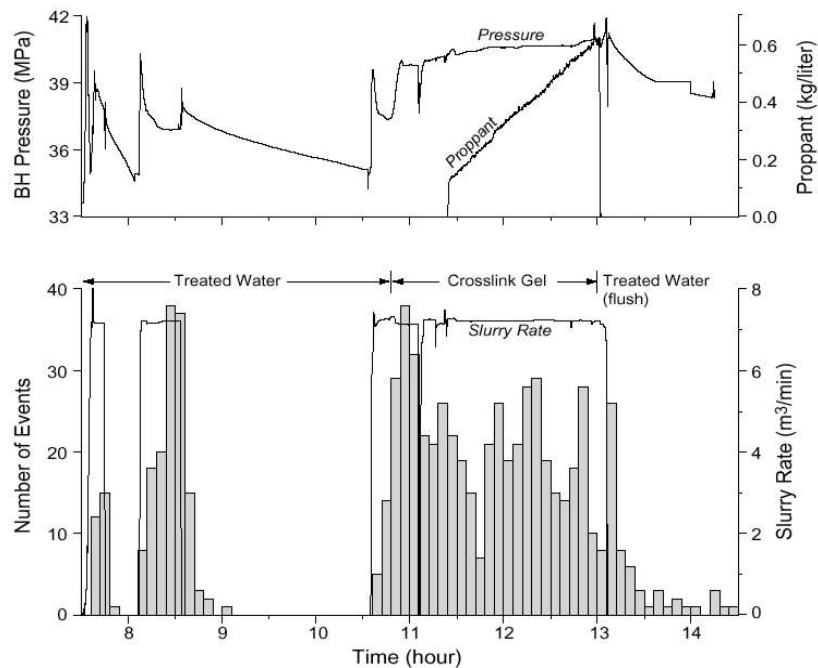


**Fig. 10:** Comparison between variations of bottomhole pressure data with time and induced microseismic event count (op. cit.).

An initial location (Fig. 11) shows that one or more fractures were actively created (or stimulated) in an east-northeast direction and that microseismicity occurs at two separate intervals within the perforated layer, with some tendency to migrate downward, stopping at the upper boundary of the zone stimulated in stage 2 hydraulic fracturing. According to the authors, it is reasonable to believe that fractures propagate symmetrically westward from the injection well. The absence of microseismicity beyond a certain distance westward is simply due to the fact that the sensors are located east of the injection well.

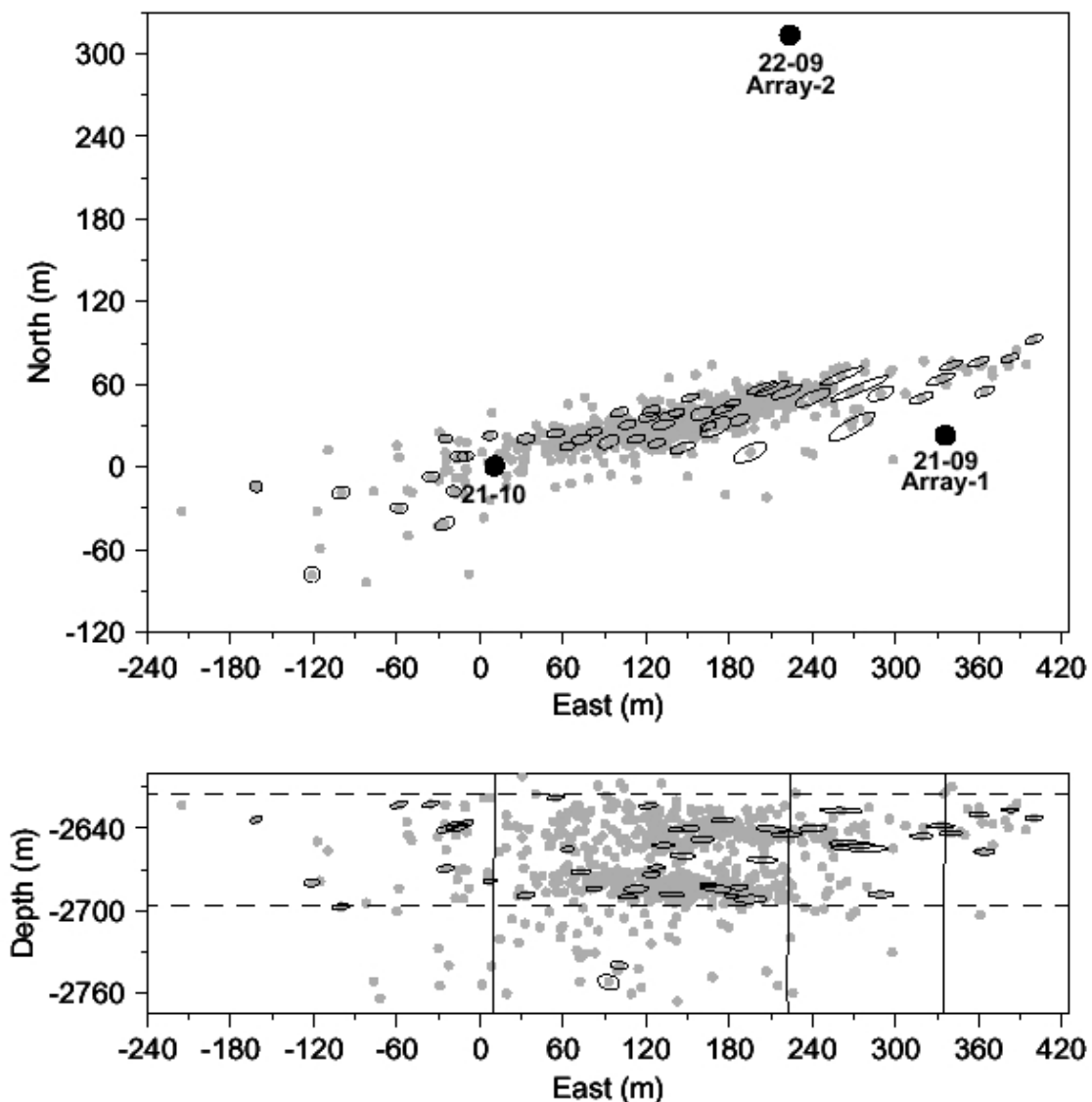


**Fig. 11: Locations of microseismicity during stage 3. Dashed lines in the depth view mark the perforated interval. Some representative error ellipsoid projections are shown (op. cit.).**

The best quality events east of the injection well were relocated simply by comparing the phases of groups of closely spaced events, following oversampling (from 1 ms to 0.2 ms) and rotation in system P (radial),  $S_H$ ,  $S_V$ . The results are startling (Fig. 12):

- the fracture zone width narrows to about 10 to 15 m;
- at least six well-differentiated intervals can be recognized on the east-west cross section;
- the median length of the principal error ellipse axes decreases from 8 m to 2 m.

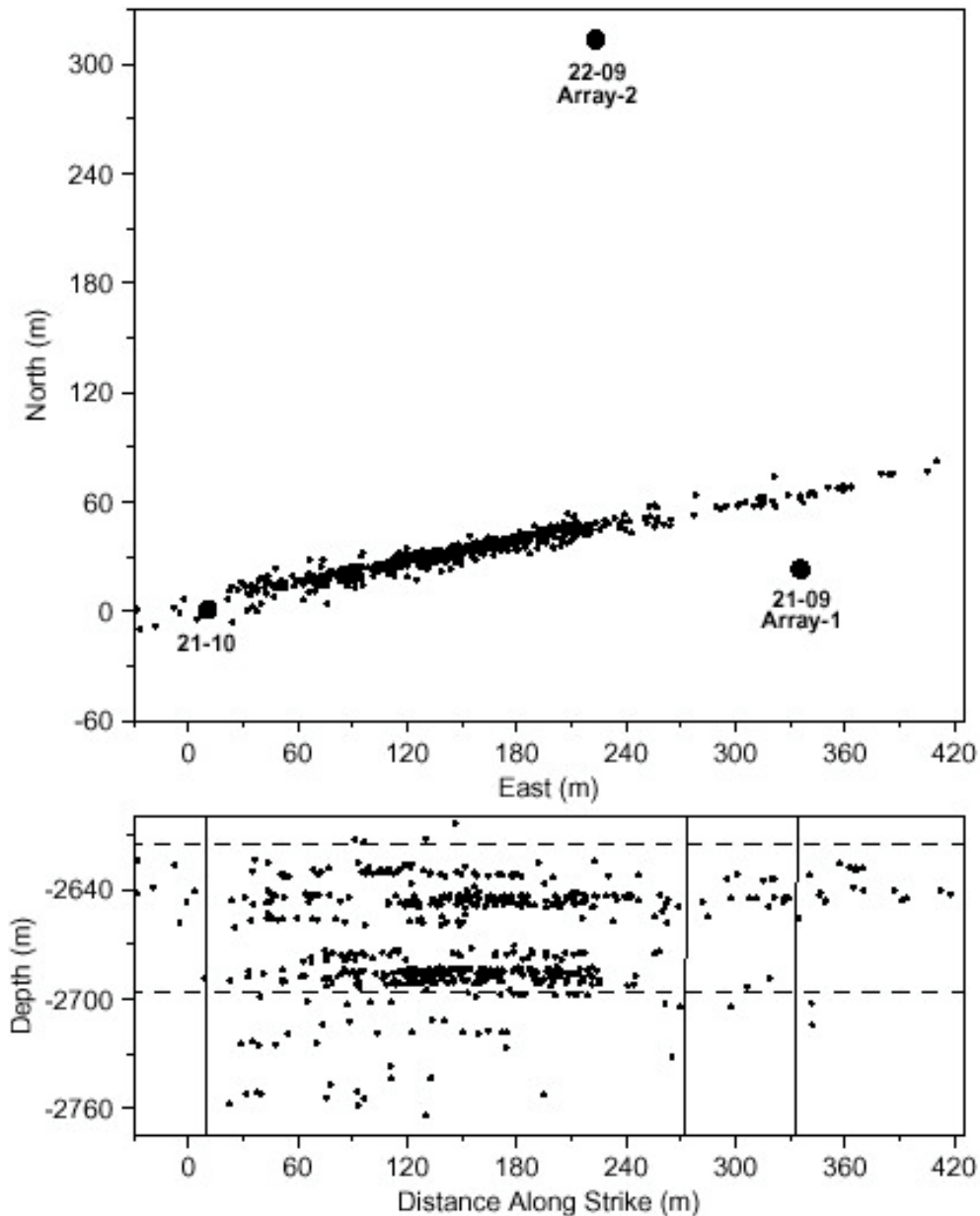


**Fig. 12:** Same as Fig. 11, after obtaining higher-precision arrival-time data.

Fig. 13 compares the histogram of the number of events with the log of a radioactive tracer injected at the same time as the proppant and the fluid. The tracer allows us to qualitatively characterize the behaviour of fractures located near the well. The stimulated sand intervals, marked A to F, appear well differentiated, both on the histogram of tracer concentration and on the histogram of the number of microseismic events. This shows that fracture height growth is relatively well contained and that there

is no microseismic evidence of communication between stimulated intervals. In addition, natural fractures are known to occur and terminate within individual sand intervals. The depth view in Fig. 8 confirms that microseismicity remains remarkably concentrated within these bands and over a considerably greater distance than the detection range of the radioactive tracer. The absence of microseismic events at interval A remains unexplained. Seismicity at intervals B and C was also observed to extend 200 m farther east than at underlying intervals. The diffuse seismicity observed below interval F, toward the top of stimulation zone 2, could be due to leakage of the fluid injected behind the casing.

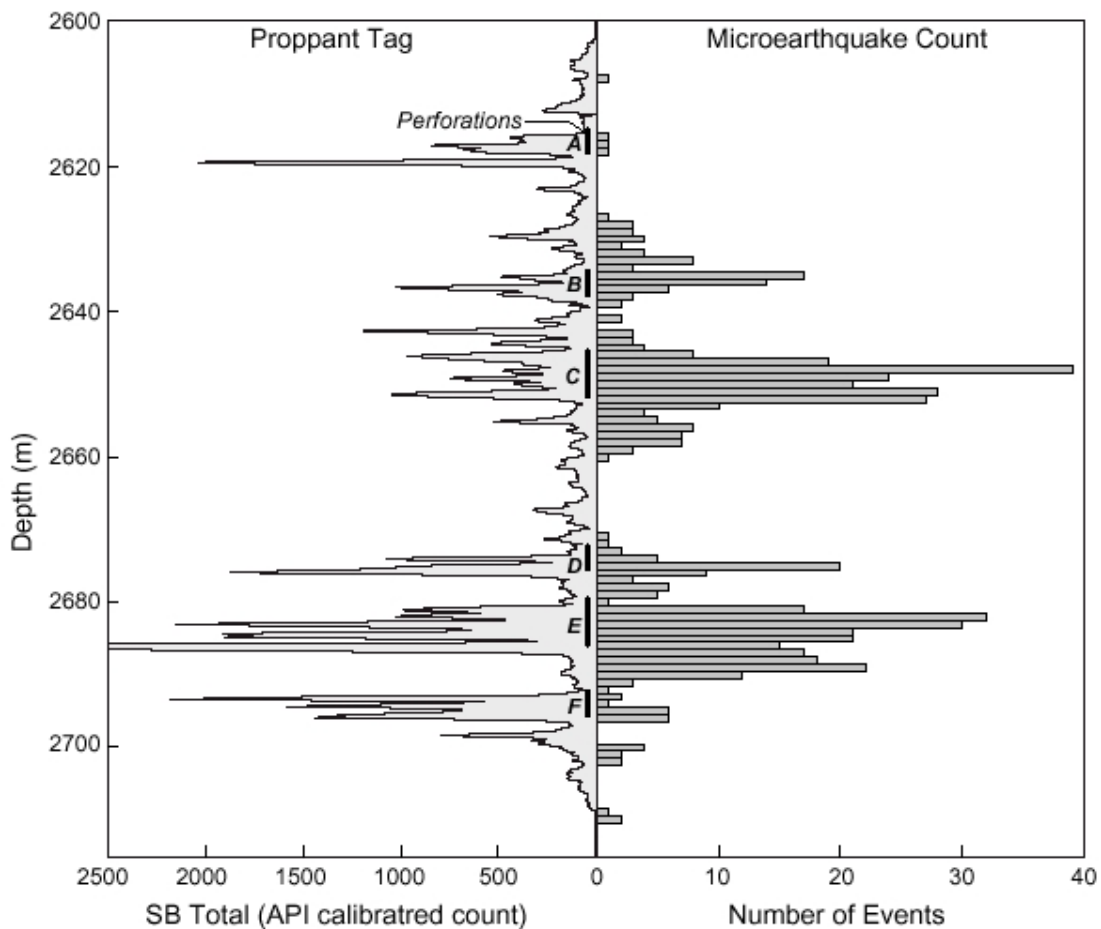


**Fig. 13:** *Comparison between the depth distribution of microearthquakes and the radioactive proppant tracer log. The dark vertical lines labelled A to F mark the exact stage 3 perforation schedule of the treatment well 21-10 (op.cit.).*

More accurate relocation highlights the systematic displacement of microseismicity that provides insight into the growth process of fractures over time. As was the case at Lower Frio (§ 1.2), movement is observed in two directions, i.e. away from and towards the injection well. The strongest events are located near the well, probably related to higher pore pressures. Strike-slip displacement must transfer shear stress in both directions, along the direction stimulated.

The calculation of composite focal mechanisms is justified for three reasons:

1. similarity of waveforms for closely spaced sources throughout the data set and over the entire fracture length;
2. consistency between  $S_H$ -wave first motions and P-polarity constrained solutions;
3. consistency between nodal planes obtained and the trend of stimulated fractures, defined by the alignment of hypocentres.

The focal mechanisms obtained (Fig. 14) are consistent with slip on the pre-existing natural fractures aligned with  $S_{Hmax}$  in an east-northeast direction. Two main groups of fractures coexist oriented  $N80^\circ$  and  $N70^\circ$ , with dextral and sinistral strike slip respectively. They are activated indifferently during periods of pumping and shut-in. Most events with a sinistral  $S_H$  first motion could be due to fractures that are aligned preferentially with  $S_{Hmax}$ .

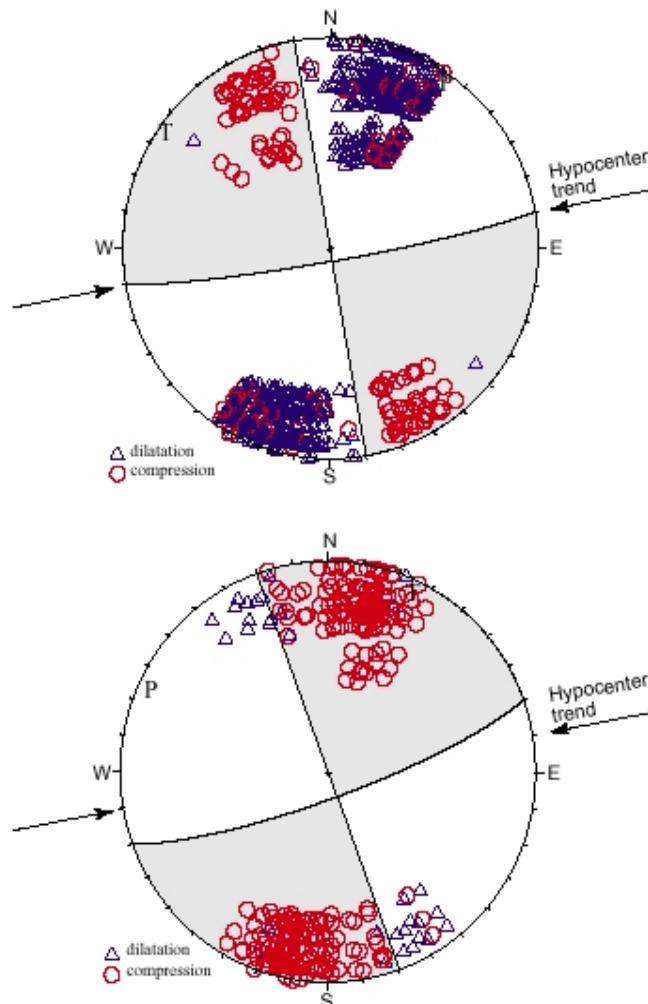


**Fig. 14: Composite focal mechanisms using P-wave first motion for two groupings of all events occurring east of the treatment well (op.cit.).**

The increase in permeability is more likely related to the stimulation of natural fractures than to the creation of hydraulic fractures. Because of their orientations, the pore pressure needed for shear slip is close to the jacking pressure. Fractures that begin to slip could be extended as hydraulic fractures with a minimal increase in injection pressure, thus improving chances of connecting subparallel fractures.

#### **1.4 THE EKOFISK OIL FIELD EXPERIMENT**

Maxwell, S.C., Young, R.P., Bossu, R., Jupe, A. and Dangerfield, J., 1998, *Processing of induced microseismicity recorded in the Ekofisk reservoir*, 68<sup>th</sup> Annual Meeting, Society of Exploration Geophysicists, 904-907.

Maxwell, S.C., Young, R.P., Bossu, R., Jupe, A. and Dangerfield, J., 1998, *Microseismic logging of the Ekofisk reservoir*, (SPE#47276), Proceedings of EUROCK'98, 387-394.

An 18-day experiment in microseismic monitoring was carried out in the Ekofisk field in April 1997 in order to study the feasibility of using production-induced microearthquakes to characterize reservoir evolution. A CGG SST500 probe, normally used for VSP (vertical seismic profiling) and composed of six triaxial geophones spaced 20 m apart, was installed at a depth between 2970 and 3020 m. Over 2100 events were recorded and the locations of 1838 of them were determined. The events were located by calculating arrival times using ray tracing and by using a grid search technique to determine the location with the best match.

The majority of events were located within 100 m around the observation well, although some were detected at 800 m and even at 2.2 km. Microseismicity is concentrated in layers having a lower porosity (<35%) than the aseismic layers (45%). It is induced by the concentration of stress in the relatively more rigid layers, due to the compaction of underlying layers as a result of oil extraction. However, zones invaded by the water in pores left by the oil seem to be aseismic. Clusters of events parallel to the dominant trend of major structural features in the zone were observed also, which suggests the reactivation of pre-existing faults. Currently, several oil companies are interested in microseismic monitoring for studying seafloor subsidence and reservoir compaction. The relationship between waterflood front advance and microseismicity is still to be determined.

#### **1.5 GEOTHERMAL FIELDS AND HYDRAULIC FRACTURING**

Induced microseismicity is a known phenomenon in geothermics and is related either to production, as with the Geysers field in California (Eberhart-Phillips and Oppenheimer, 1984), or to the reinjection of fluid withdrawn to maintain pressure in a reservoir or for environmental reasons, as with the Geysers field (Rutledge *et al.*, 2000) and Cerro Prieto in Mexico (Fabriol and Munguía, 1997). Passive seismic monitoring has been the most commonly used, and the most striking developments in data processing and

interpretation have been made, during Hot Dry Rocks<sup>1</sup> projects. From the cases described in the literature, we present those of Fenton Hill (New Mexico) and Soultz-sous-Forêts (Alsace, France).

At Fenton Hill, over 21,000 m<sup>3</sup> of fluid were injected in 61 hours at a depth of 3460 m into granitic basement under a recent volcanic caldera (Phillips *et al.*, 2000). Downhole instrumentation included two x vertical-component sensors at a depth of 500 m near the top of the basement and two x three-component (high pressure, high temperature) sensors at depths of 2855 m and 3300 m. Over 11,000 events were recorded and located in a tabular volume approximately 1 km by 1 km by 300 m. Precise relocation techniques were applied to selected clusters within the microseismic cloud, which resulted in a marked decrease in scattering of hypocentres and the appearance of spatially limited planes in which events were grouped in clusters. The authors suggest that these 'seismic' planes are slip planes, bounded by aseismic joints that are part of the fluid-flow network.

The European HDR project at Soultz-sous-Forêts is still under development. The present-day reservoir is located in granitic basement at depths between 2 km and 5 km (Phillips *et al.*, 2000). The 1993 experiment injected 44,000 m<sup>3</sup> at a depth of 2850 m, which generated over 16,000 microearthquakes. The measuring device comprised three x four-component sensors and one hydrophone at depths between 1.3 km and 2.1 km. As at Fenton Hill, the microseismic cloud has a vertical tabular shape approximately 1.5 km by 1.1 km by 0.5 km, and was roughly parallel to the direction of the maximum horizontal stress. A number of papers were published about cluster relocation using different methods, and focal mechanisms were determined. The progression of seismic activity over time along linear segments allows microseismicity to be linked to permeable zones within the fractures. Channelling of flow in these narrow conduits corroborates the modelling predictions.

## 1.6 CONCLUSIONS

Table 1 summarises the characteristics of the various oil fields in which microseismicity was observed and provides additional examples from the literature that we consider important (see References), particularly the Vacuum Field in the USA, where an experiment in EOR using CO<sub>2</sub> injection was followed by passive seismic work. Over 2000 microseismic events were recorded, several hundred of which were located (B. Schuessler Mayer, pers. comm.). The high number of events is probably related to the relatively low porosity of the limestones (approx. 12%), a permeability of 22 mD and the substantial increase in reservoir pressure (from 11.6 to 17 MPa) following injection (Liu *et al.*, 2001).

We begin by recognizing that numerous mechanisms generate induced microseismicity: gas storage, EOR using CO<sub>2</sub> or hydraulic fracturing, fluid injection, production-related reservoir compaction, etc. Although the low porosity of carbonates and sandstones is a

---

<sup>1</sup> HDR projects involve creating a reservoir by hydraulic fracturing and circulating a fluid in it to recover heat.

contributing factor in the occurrence of hundreds of microearthquakes, examples of high-porosity environments (Lower Frio and Ekofisk) show that this is not the only trigger. However, the first example involves fluid injected into sandstone and the second, production-related compaction. Clearly, other factors are also favourable: high injection pressures, the use of fluid and/or proppants, the stress regime. Fractures or faults are supposed to be critically stressed in a compressive stress regime. However, the number of events recorded is relativized by the distance between the source and the measuring device

**Table 1: Comparison between different historical cases of induced microseismicity**

Field	Lithology	Treatment	Depth (m)	Porosity (%)	Stress regime	Natural fractures	Injection pressure or pore pressure variation in the reservoir (MPa)	Total number of micro-earthquakes	Maximum source-receiver distance (m)
Germigny-sous-Coulombs	Sand and sandstones separated by shales	Gas storage	800-900	20		No	1.5 to 2.5 $\Delta\sigma = 0.04$ to 0.1 above reservoir)	27	75
Vacuum Field	Carbonates	EOR with CO <sub>2</sub> injection	1500	11.6		Yes	$\Delta\sigma \approx 6$ MPa	> 2000	150
Lower Frio	Sandstones bounded by shales	Fluid injection (8000 m <sup>3</sup> ) for solid waste storage	1349-1407	High permeability		No?		2900	200
Cotton Valley (Stage 3)	Tight gas sands within interbedded sequence of sands and shales	EOR, hydraulic fracturing (1253 m <sup>3</sup> of water + proppant)	2600-2700	9.3	Extensional	Yes	About 40 MPa bottomhole	1122	500
Cotton Valley (Stage 2)	Idem	Idem (1100 m <sup>3</sup> of water)	2757-2838	9.3 (?)	Extensional	Yes		~1200	500
Giddings	Austin chalk	EOR, hydraulic fracturing (two phases: 4000 m <sup>3</sup> , water + acid)	2100-2350	5 to 8		Yes	Up to 21 MPa (wellhead)	480 770	700
Clinton County	Carbonates	Production/stress concentration by compaction + brine invasion	230-730	2 to 7	Compressive	Yes	$\Delta\sigma \approx 0.02$	3200, six weeks after a nearby well began production	Up to 700
Ekofisk	Sandstones	Production/stress concentration by compaction	2930-3020	< 35 for low porosity layers	Compressive	Yes		2100 within 18 days	800
Sleipner	Sand and sandy shales	CO <sub>2</sub> injection	800-900	27 to 40	Compressive	In shales?	$\Delta\sigma < 0.02$	?	?

## 2. Data acquisition and processing

### 2.1 GENERAL

In most known examples, induced microseismicity involves suites of numerous small events with a magnitude range of -4 to -2, the largest ones not surpassing +1. This behaviour is similar to that of earthquake swarms or volcanic sequences that are consistent with heterogeneity in stress and permeability distribution. These events must therefore be recorded from wells located as closely as possible to the injection zone. This has the advantage of avoiding scattering and attenuation problems due to near-surface soil layers.

Clamping and cementing of the sensor to the well wall must be of good quality. A poor bond can lead to parasitic resonance, which renders waveforms unusable. Three-component geophones are essential for processing shear waves.

To accurately locate events, at least two x three-component geophones must be used in different wells. Since the latter half of the 1990s, most recordings have been made using multilevel devices, with geophones spaced a few metres to a few tens of metres apart. Instead of requiring several wells, a string of several sensors deployed at different levels can be used within a single well.

Sensor calibration is crucial for the location of microearthquakes. P- and S-wave velocities are generally well known from sonic logs. Calibration shots are needed to determine precise geophone orientation and station corrections. These corrections enable velocity models to be adjusted from an accurate knowledge of sensor and shot positions.

### 2.2 SENSORS AND RECORDING SYSTEM

Our example uses tools available on the market. Two types of systems are possible (Fig. 15): wireline monitoring tools and permanent or semi-permanent tools

#### 2.2.1 Wireline monitoring

The CGG SST-500 VSP tool was used at Ekofisk and at Vacuum Valley. This tool is normally used for VSP<sup>2</sup>. At Vacuum Valley, it was used to record microseismicity outside of periods of recording active seismicity. It can include up to six levels of three-component sensors spaced 15 to 20 m apart<sup>3</sup>. A hydraulic system is used to clamp the sensors to the tubing. Data digitization (24 bit resolution, 1 kHz sampling frequency) is done downhole, and a seven-conductor cable can be used to bring up the information.

---

<sup>2</sup> The OYO company proposes similar tools for VSP; these tools can also be used on a temporary basis for microseismic monitoring.

<sup>3</sup> At Vacuum Field, the downhole array included 10 levels.

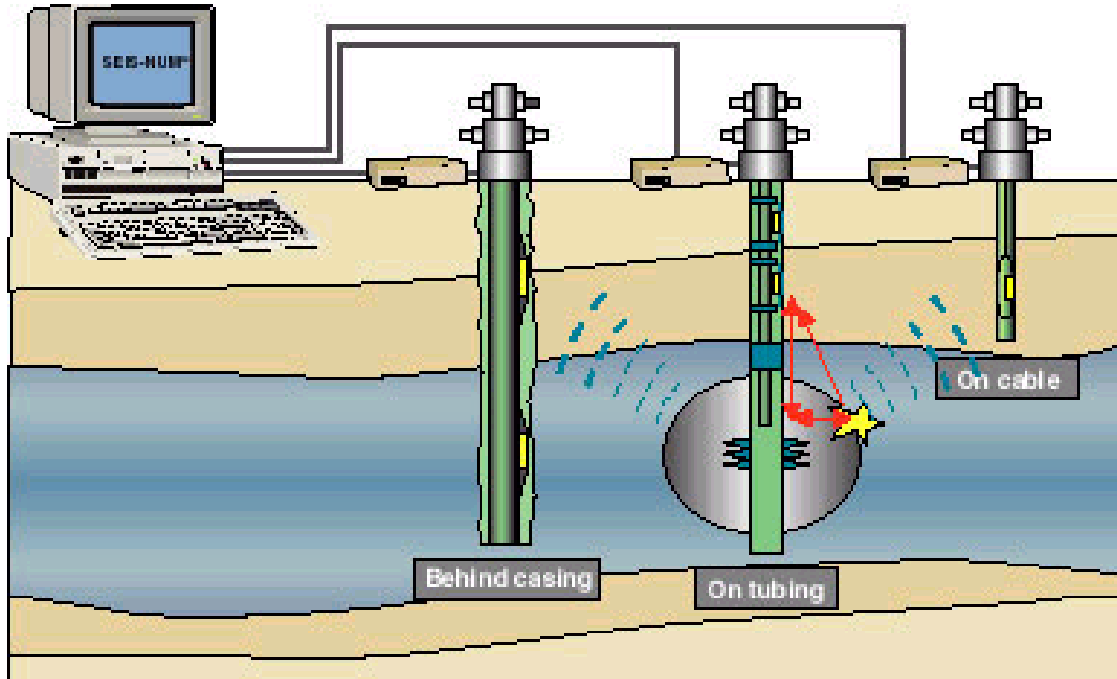


**Fig. 15: Different examples of downhole monitoring (source CREATECH Industrie).**

CGG also proposes the MSR-600 tool, specially developed for seismic monitoring in a semi-permanent installation. An electromechanical system is used to clamp the tool to the well, which permits a flat sensor response up to 600 Hz. Four triaxial sensors can be deployed on a single cable with a maximum spacing of 50 m. The downhole digitization system (maximum sampling frequency of 2400 Hz) is designed in such a way that the MSR-600 can be used with classical wireline as well as with a single wireline conductor. It has a diameter of 2¼", which allows it to be used in wells from 2½" to 6½".

CGG also provides PC acquisition and processing software in the same package.

Another option is the SIMFRAC™ system from IFP (Figs. 16 and 17), which includes a triaxial accelerometer, pressure and temperature gauges and high-rate digital telemetry (2 kHz for seismic signal and 1 Hz for pressure-temperature). It is specifically designed for hydraulic fracture mapping and fluid injection monitoring during the minifrac operation. It can be used through tubing larger than 2½" and casing up to 9 5/8". The SIMFRAC™ probe is lowered by wireline (single wireline conductor) into the well, below the perforation or injection zone two permanent magnets are used to clamp the seismic sensor module to the casing. Together with the downhole acoustic probe, the

surface acquisition unit (PC based) allows processing of microseismic data, fracture mapping and correlations with injection parameters (SIMFRAC-MAP™ software).

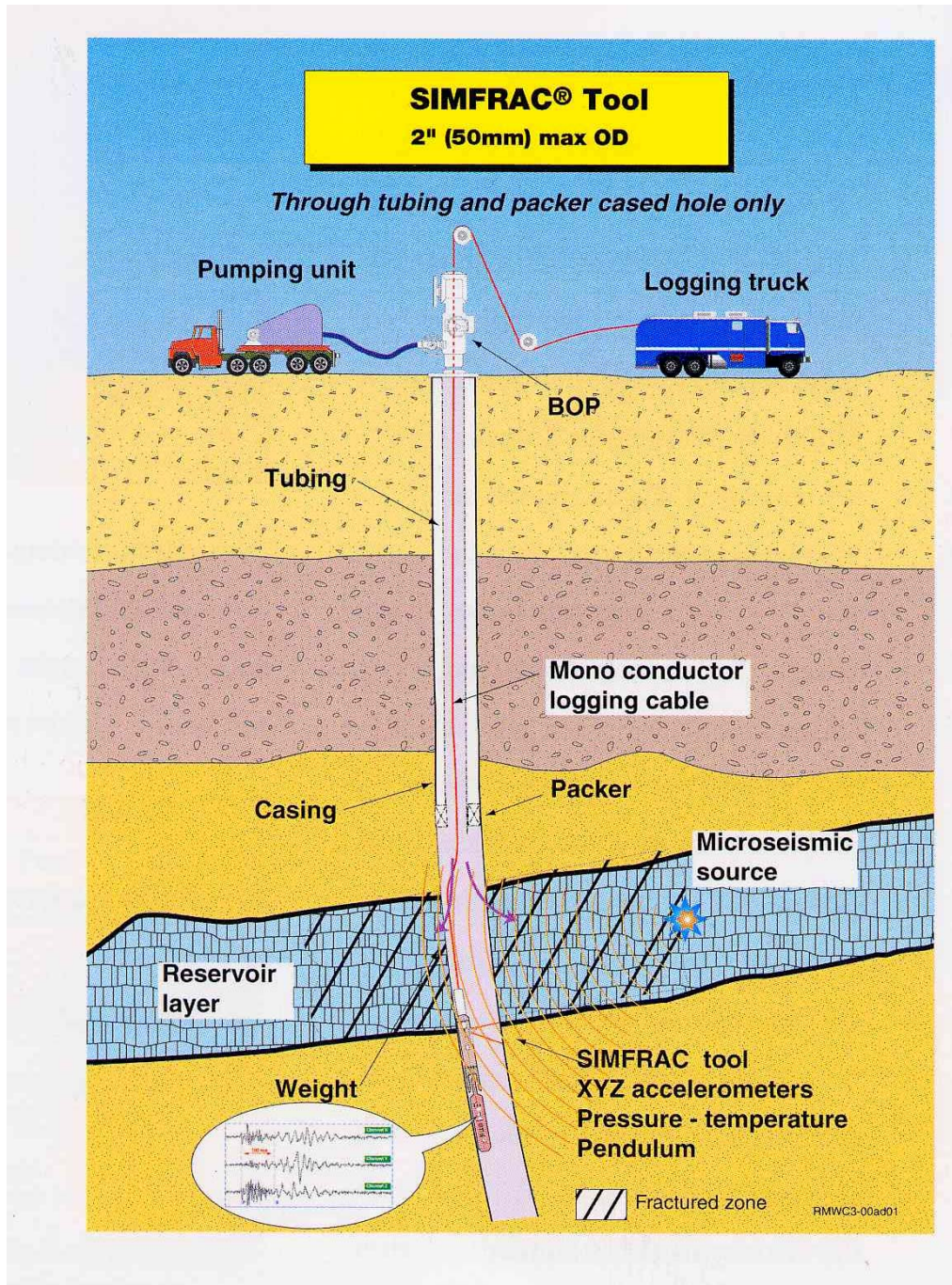


Fig. 16: IFP SIMFRAC™ tool

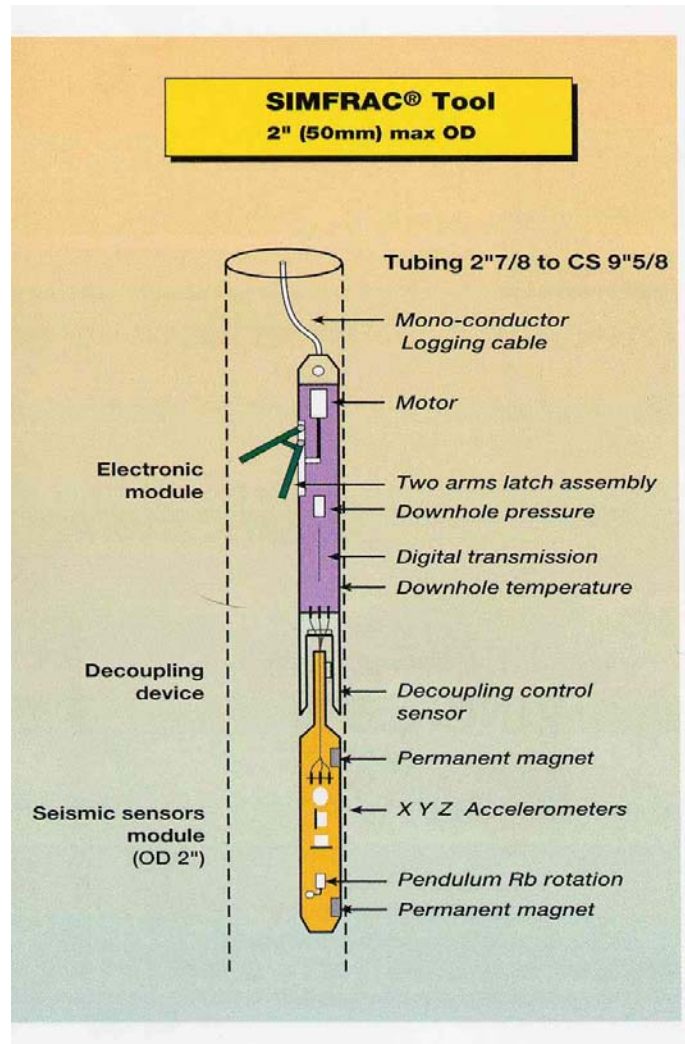


Fig. 17: IFP SIMFRAC™ tool installation diagram

### 2.2.2 Permanent monitoring

The other technology used involves sensors permanently installed between the tubing and the casing or behind the casing. The entire array is installed on the tubing (or casing) as it is lowered into the well. The tool's principle is roughly the same as that of the wireline: downhole HF multichannel digitization module, three-component sensors, possibility of using a single-conductor cable to bring up the information, etc. However, clamping to the casing is different and can be done using a mechanical system<sup>4</sup> or by cementing (for installation behind the casing). For sensors cemented behind the casing, the entire system is bolted to the casing before it is lowered into the well. Later cementing of the casing ensures the best possible bond.

<sup>4</sup> The electromechanical option is not recommended as it requires a continuous supply of electrical energy from the surface.

For installation between the tubing and the casing, CREATECH Industrie<sup>5</sup> proposes an integral system that uses a spring leaf to bond the sensor to the casing (Fig. 18). The annular space required between tubing and casing is minimized (for example OD 6 5/8" tubing and ID 9 5/8" casing). The sensor's bandwidth is greater than 1 kHz.

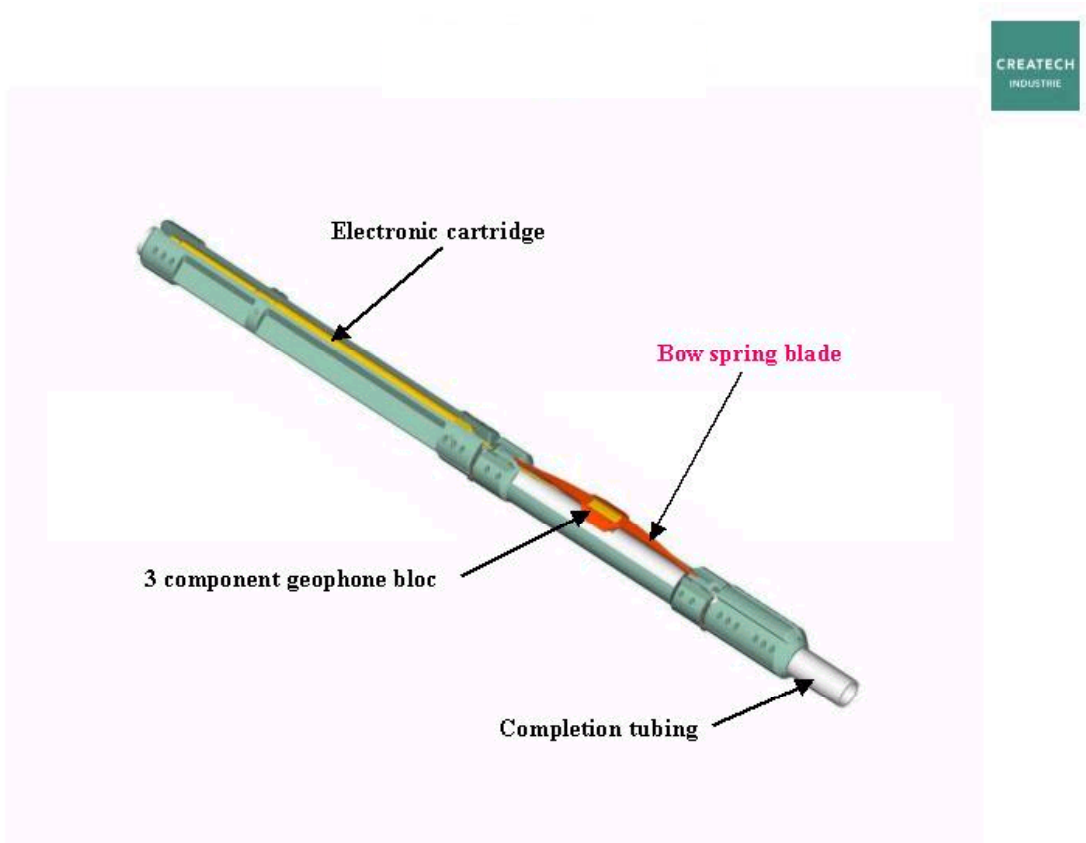


**Fig. 18:** *Permanent microseismic monitoring probe placed between tubing and casing (source CREATECH Industrie).*

At Cotton Valley, two strings 715 m long, comprising 48 x three-component geophones spaced 15 m apart, were fixed to the 2 7/8" tubing, then lowered into and cemented onto the casing in two different wells. Signals were amplified 1000 times downhole, then digitized at the surface (sampling frequency of 1 kHz).

Other references to passive seismic monitoring systems can be found in:

Albright, J.N., Rutledge, J., Fairbanks, T.D., Thomson J.C. and Stevenson, M.A. (1998), *Vertical Array for Fracture Mapping in Geothermal Systems*, Transactions, Vol. 22, Geothermal Resources Council Annual Meeting, 20-23 September 1998, San Diego, California, pp. 459-463.

<sup>5</sup> CGG and IFP propose similar systems that use the CREATECH sensor.

## 2.3 LOCATION METHODS

The classical method involves the inversion of P- and S-wave arrival times at different sensors. For a location precision of the order of tens of metres or better, two conditions must be met:

- A minimum sampling frequency of 1 kHz, the frequency of recorded signals varying from about 100 to 500 Hz. This is no longer a problem thanks to downhole digitization.
- An accurate reading of arrival times. For now, the visual method provides better results than automated techniques. Repicking of first peaks was used for signals from Cotton Valley (Rutledge and Phillips, 2001).

Proximity and similarity of sources and common paths commonly result in very similar waveforms. This can be used to:

- stack waveforms of events whose sources are considered to be almost spatially merged in order to enhance emerging P arrivals (Vacuum Valley example, B. Schuessler, pers. comm.);
- apply methods of cross-correlation between waveforms of closely spaced events, in order to calculate relative arrival times rather than search for the first break on each seismogram (doublet/multiplet method).

Hodograms were widely used before the appearance of sensor strings, when only one or two three-component sensors were available. They involve determining the azimuth of propagation of the P-wave from the polarization of the arrival first peaks on a triaxial geophone. The source-receiver distance can be estimated from the S-P difference. The main inconvenience is the poor knowledge of sensor orientation and the possible appearance in first arrival of refracted rays in structures with three-dimensional geometry, which distorts the location. Hodograms are currently used mainly to constrain arrival time inversion.

The doublet or multiplet method is based on the principle that events whose sources are very closely spaced have similar waveforms (Poupinet *et al.*, 1984). The relative location of secondary events is determined with respect to a master event whose location is known with precision. The differences between first arrivals are calculated by a cross-correlation technique with a resolution better than the sampling frequency; thus relative locations can be calculated with an accuracy better than one metre. This method has been used successfully to determine fracture planes or earthquake alignments along faults.

Other methods can be used to increase location precision:

- Joint hypocentre-velocity inversion adjusts all combinations of P- and S-wave velocities, station corrections, geophone orientations and hypocentre locations so as to best match observed data, arrival times and hodogram data (Phillips *et al.*, 1998a).
- The joint hypocentre determination (JHD) method allows the calculation of station corrections that compensate for uncertainties in the P- and S-wave

velocity model, by ultimately integrating hodogram data (B. Schuessler, pers. comm.).

- The master event technique selects the event considered to be the most accurately located on the basis of the number and quality of its arrival times and reintroduces residual times (difference between observed times and calculated times at each station) as station corrections in the subsequent location step. These corrections are then adjusted in such a way that residual times approach most closely RMS residual times for the entire data set (Phillips *et al.*, 2000).

Research is also focused on the search for details in microseismicity clouds. The three-point method of Fehler *et al.* (1987) is used to find the orientations of planes by systematically searching for all possible combinations of three hypocentres taken individually. The collapsing method (Jones and Stewart, 1997) involves reducing location errors for closely spaced hypocentres by concentrating them on their centroid (Fig. 19). The positions and orientations of planar features found by the collapsing method are comparable to those obtained by a precise repicking of arrival times (Fehler *et al.*, 2000).

In some cases, the combined use of several sensors and P and S first arrivals allows composite focal mechanisms to be determined by involving a large number of closely spaced events (see the Cotton Valley example, Fig. 14). The orientations of fracture planes and stress axes so determined are compared with other known data, i.e. alignment of microseismicity planes, downhole determination of stress tensor, analysis of oriented cores, etc.

The very large quantity of data (several hundred to several thousand events) requires the use of automated methods for determining arrival times and hypocentres. However, such methods have yet to produce results as good as those obtained manually. This is due to the fact that the similarity between waveforms from closely spaced events is not always adequate because of very localized variations in source-receiver paths or because of the state of stress near the source.

Finally, interpreting microseismicity from reliable locations of seismic sources involves:

- analyzing their evolution in time and space in order to identify preferential flow planes or axes;
- searching for correlations with the course of the operations and variations in pressure-flow parameters (insofar as they can be measured).

As an example, the  $\mu$ SICS™ software from IFP (Deflandre *et al.*, 2001) combines basic processing of microseismic data with the management of a database that includes most of the different parameters related to:

*1- Microseismicity:*

- waveform analysis, spectra, amplitudes;
- hypocentre determination;

- source parameters.
- 2- *Site information:*
  - geology;
  - mechanical properties;
  - logging, etc.
- 3- *Injection monitoring:*
  - pore pressure;
  - fluid pressure;
  - flow;
  - fluids geochemistry, etc.

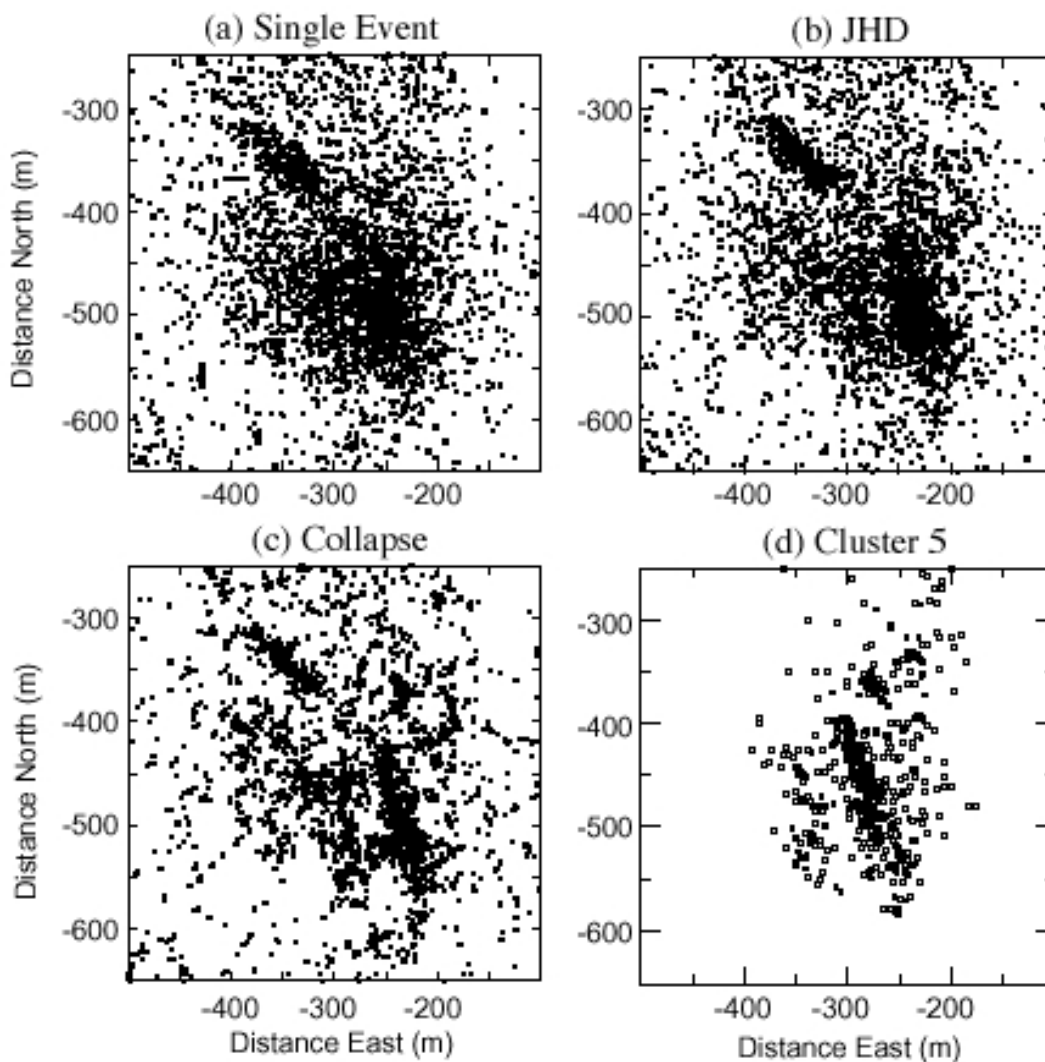


**Fig. 19:** *Location of Fenton Hill events within a cube having 400-m sides; (a) locations from the single-event location method, (b) JHD locations, (c) locations from the JHD-collapsing method, (d) locations using relative arrival time picks for the subset of events exhibiting similar waveforms (from Fehler et al., 2000).*

The objective is to characterize each event or group of events using as many deterministic parameters as possible. Following this,  $\mu$ SICS™ suggests two methods of classification of events to link particular space-time sequences of seismic events with distinct features of the reservoir behaviour (CO<sub>2</sub> front progression, reopening of natural fractures, i.e. mainly strike-slip displacements, CO<sub>2</sub> flow through aseismic areas, etc.).

## **2.4 CONCLUSIONS**

Given the magnitude of microearthquakes, downhole sensors must be located less than a few hundred metres from the sources. Tools consisting of 12, 24 or 48 x three-component sensors are now commonly used for semi-permanent observations lasting a few months. Sensors permanently placed between the tubing and the casing or cemented behind the casing can be used in a permanent network. Over the past few years, geophysical and wirelogging companies (CGG, ABB, Magnitude, etc.) have provided data acquisition and processing services. Methods for processing huge masses of data have greatly improved and software is readily available for purchase.



### 3. What could be expected at Sleipner

The following are the principal causes of induced seismicity in a reservoir in which there is fluid movement:

- the natural state of stress due to the geological setting;
- the mechanical properties of the reservoir rocks and host rock;
- the changes in pore pressure due to fluid withdrawal or injection.

This chapter presents a literature review of the state of stress in the North Sea as well as observations on the occurrence of microseismicity.

#### 3.1 SEISMOLOGICAL DATA

According to Bungum *et al.* (1991), the offshore Norway seismic activity is confined to the fault zone corresponding to the western margin of the Viking Graben (Appendix 1). The largest known historical earthquake is the North Sea earthquake (magnitude 5.1 to 5.3) that occurred on 24 January 1927 at about 59°N, 2.5°E (event 1 in Fig. 20). Its focal mechanism is unknown. According to data from Bungum *et al.* (1991), focal mechanisms of two earthquakes (magnitude close to 4) that occurred north of Sleipner at 60.40°N and 61°N respectively showed strike-slip and reverse faulting (events 2 and 3, fig. 20). Three earthquakes that occurred farther north (events 4 to 6, Fig. 20), with magnitudes of 4.5, 3.1 and 4.9, respectively, showed reverse faulting in response to northwest-southeast compressive stress.

#### 3.2 DOWNHOLE MEASUREMENTS

Data relating to stress orientation, minimum principal stress and pore pressure have been obtained from borehole breakout data, drilling-induced tensile fractures and leak-off tests carried out over the entire Norwegian sector of the North Sea. Measurement density south of 59°N is less than in the northern sector. The average orientation of  $S_{Hmax}$  (maximum horizontal stress) in the Central Graben is estimated to be approximately 97° from borehole breakouts (Gölke *et al.*, 1996), and NNW-SSE from drilling-induced fractures (Grollmund *et al.*, 2000).

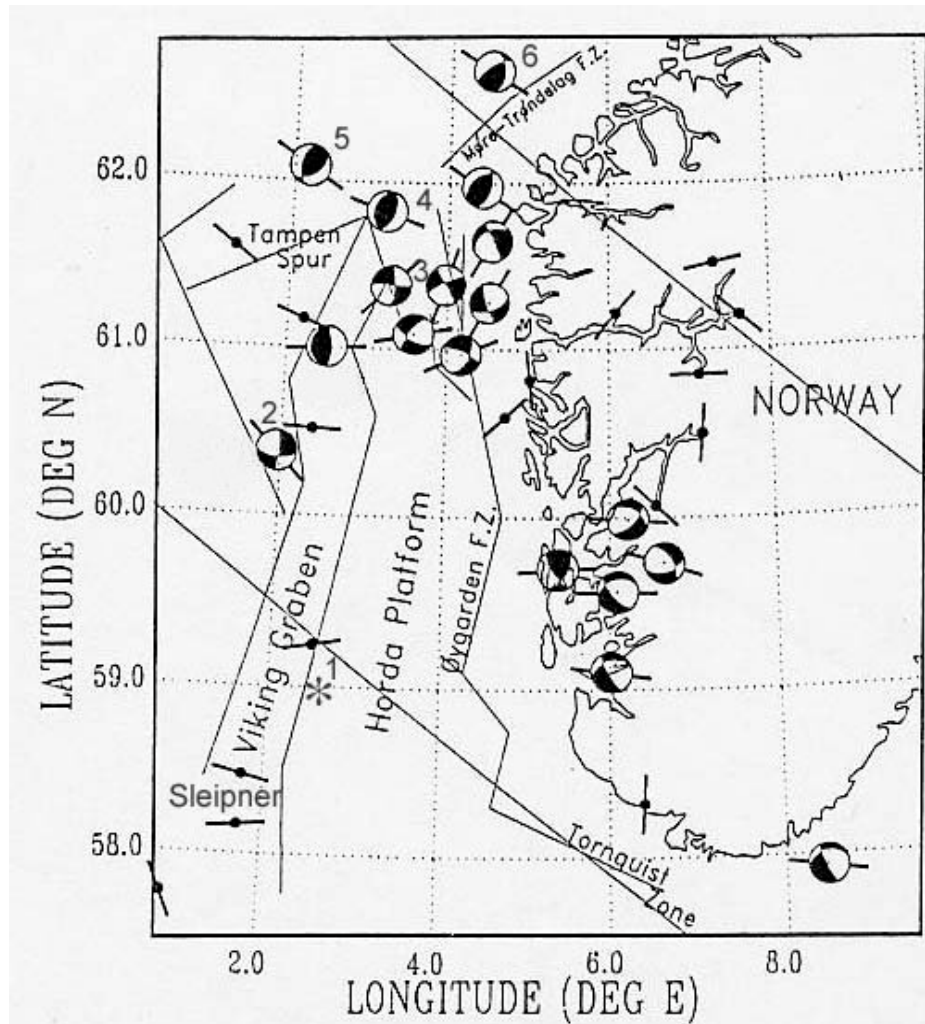


**Fig. 20:** *Focal mechanism and in situ stress measurement (solid circles) in Western Norway and in the Northern North Sea. Details about events 1 to 6 are given in the text. The lines through the focal sphere projection indicate the direction of P axes (maximum compressive stress). The two parallel NW-SE trending lines across the map are “ridge push” or flow lines computed on the basis of a spreading pole at 52°N, 12.9°E. FZ = fault zone (from Bungum *et al.*, 1991).*

The stress regime in a selected area can be determined from the  $S_3/S_V$  ratio, equivalent to  $S_{Hmin}/S_V$ .  $S_V$  is the vertical stress (lithostatic) calculated from density logs. An  $S_3/S_V$  ratio  $<1$  corresponds to a normal faulting (extensional) regime, and an  $S_3/S_V$  ratio of nearly 1 to a reverse faulting (compressive) regime. An  $S_3/S_V$  ratio  $\approx 1$  can represent a nearly isotropic stress state in which the viscous behaviour of Plio-Pleistocene sediments leads to an almost immediate relaxation of any external differential stress, such may be the case at Sleipner. Grollimund *et al.* (2000) present plots (Fig. 21) in which  $S_3/S_V$  seems to be between 0.95 and 1 in the Sleipner region at depths between 1500 m and 3000 m, indicating a compressive (strike-slip or reverse faulting) stress state.

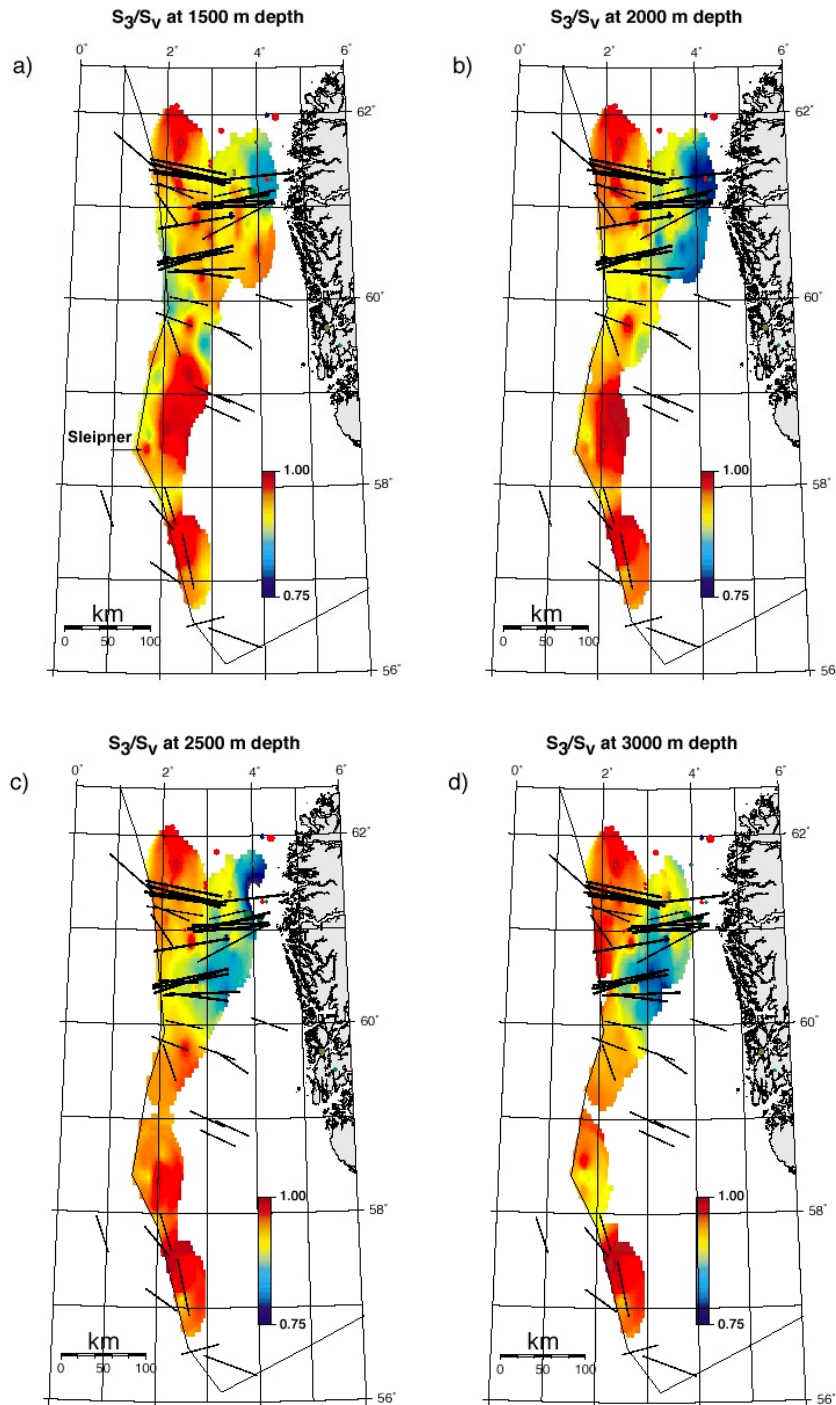


**Fig. 21:** *Lateral variations of the least principal stress normalised by the vertical stress ( $S_3/S_V$ ) for different depth slices.  $S_3$  is derived from leak-off tests and  $S_V$  comes from the integrated density logs. The Fig. shows that  $S_3/S_V$  is consistently low close to the Norwegian coast and increases towards the west (perpendicular to the coastline). The black lines indicate  $S_{Hmax}$  orientation (from Grollmund et al., 2000).*

In the same paper, Grollmund *et al.* (2000) mapped pore pressure at various depths from measurements taken in 385 wells in the Norwegian sector of the North Sea. For the Sleipner area, pore pressure is hydrostatic to approximately 2000 m below sea level. According to the authors, this is not surprising given that pore fluids are likely to be in hydraulic communication with the seafloor as a result of increased permeability. That contradicts available information from CO<sub>2</sub> storage at Sleipner, since no leaks were observed up to now. A moderate overpressure is observed between 2000 m and 3000 m depth, as is the case in other sectors of the North Sea.

### 3.3 ORIGINS OF THE PRESENT-DAY STRESS FIELD IN THE NORTH SEA

According to Grollmund *et al.* (2000), the regional stress field in the North Sea is the sum of several effects:

- Ridge push associated with cooling of the crust and its increasing density as it moves away from the Mid-Atlantic Ridge. This causes an increase in horizontal stress in the direction of plate motion.
- Lithospheric bending due to the rapid deposition of Tertiary sediments, whose weight increases horizontal stress in the upper parts of the crust, which may explain local stress variations.
- Strike-slip stress through the continental margin due to differences in density between continental crust and mantle, which results in the production of compression in oceanic regions and tension in continental regions.
- Isostatic response to deglaciation, which produces extension (decrease in horizontal stress) in continental regions and compression in oceanic regions (increase in horizontal stress at shallow depths).

Wiprut and Zoback (2000) have dedicated a publication to a normal fault in the Visund oil field, along the western wedge of the Viking graben. They show that, if natural gas accumulates in a permeable reservoir bounded by a sealing fault, the pore pressure at the fault-reservoir contact increases because the pressure gradient in the gas is considerably less than the hydrostatic gradient, owing to the extremely low density of the gas. In this particular case in the North Sea, where a compressive stress state is observed (see above), the fault may be reactivated should the pore pressure reach the critical pressure (in the order of 1 to 7 MPa) needed for Mohr Coulomb failure and should the fault be oriented optimally with respect to the existing state of stress, i.e. perpendicular to  $S_{Hmax}$ .

### 3.4 CONCLUSION

The following conditions could promote seismic slip along natural faults or fractures at Sleipner:

- the regional compressive stress regime, because of which faults, whether present and depending on their orientation with respect to  $S_{Hmax}$ , can be critically stressed fractures;

- the slight overpressure due to injection of CO<sub>2</sub>, which is added to the hydrostatic pressure. Carlsen *et al.* (2001) predict an overpressure of 0.02 MPa due to the accumulation of CO<sub>2</sub> in the space confined by the caprock;
- examples of triggering of failure for stress variations as slight as 0.02 MPa (in a compressive regime), from King *et al.*, 1994.

However, these conditions are offset by the following:

- mechanical characteristics below 1500 m depth: according to Grollmund *et al.* (2000), sediments are not sufficiently consolidated to support an external stress, which is in keeping with porosity values over 27% and permeability values over 1D in the Utsira Formation;
- the question of whether faults actually do exist in and above the Utsira Formation. A priori, the apparent structures are due to mud volcanoes and intraformational faults are more likely to affect the underlying Oligocene sediments (as in the Troll field northeast of Sleipner).

As a rule, the injection of CO<sub>2</sub> in sands of the Utsira Formation should not trigger any measurable microseismicity except in impermeable or semi-permeable shale lenses that block the rise of CO<sub>2</sub> toward the top of the formation. This could be an indication of the presence of CO<sub>2</sub> insofar as it would allow the detection of conduits used for CO<sub>2</sub> migration. The start of this passage still has to be established in order to define the advance of the CO<sub>2</sub> front. Similarly, microseismicity may appear at the top of the formation. This could be evidence of the initiation of open fractures that could subsequently give rise to leakage.



## 4. Proposals for a field experiment

The previous chapter concludes that induced microseismicity is unlikely to be observed at Sleipner; it is therefore recommended to first verify the existence of microseismicity. This could be done at a marginal cost through the use of an observation well.

This chapter is based on the report “Monitoring well scenarios”, from the SACS-2 Work package 4 (Carlsen *et al.*, 2001), which presents various arguments for drilling one or two vertical offshore wells:

1. the first in the gas cloud above the injection point;
2. the second in one (or several) aquifers connected to the Utsira Formation, but not yet reached by the gas. This second well would be permanently equipped with instrumented tubing.

The observation well would be used for:

- providing direct access to the hydraulic and mechanical parameters of the reservoir and its cover;
- verification of the presence of the CO<sub>2</sub> bubble at a location where 4D seismics and/or modelling has detected (well 1) or predicted (well 2) its future presence;
- *in situ* calibration of parameters used in 4D seismics and hydrodynamic modelling.

The report also mentions the possibility of deploying seismic sensors in well 2 to complement surface instruments that measure active seismicity, even though Carlsen *et al.* (2001) are not very optimistic about the existence of microseismicity. This geophone string would be used for repeated VSP, particularly during 4D seismic surveys. Should the option selected be the observation well with seismic sensors, we recommend the addition of a system for continuously recording signals. This is the best way to verify, at a marginal cost, whether or not microseismicity exists.

The type and mode of installation of permanent sensors are described briefly in chapter 2.2. The Work package 4 report also provides an example (CREATECH material set up by CGG) and makes reference to Halliburton.

The cost of the surface recording system would be in the order of 20,000 EUR. Its design and installation should preferably be entrusted to the company that will install the permanent seismic sensors. The cost of the system used for transmitting data from the specially outfitted wellhead to the platform on which the system will be located, should be included in the overall financing of the permanent seismic system planned for 4D seismics. Data collection and processing can be done by a land-based operator who will interrogate the recording system periodically using the Internet and carry out routine processing with, for example, a weekly or monthly bulletin on microseismic activity.

The following table provides an idea of the cost of such a set up (proposal from Magnitude using CREATECH material). The last three items correspond to the additional cost of a continuous recording system with data processing for one year, that is to say 92,000 €. A proposal from Magnitude details in Appendix 2 follow up of the seismic network and design, setting and periodical update of the automatic monitoring procedures. The monitoring software allows automatic location of events.

Cost of a 3-component 12-level tool	500,000 €
1000 m of 'encased' single-conductor cable	11,000 €
Installation and testing of the device*	300,000 €
Continuous recording system	20,000 €
Setting up monitoring procedures and automatic analysis software (step 1+2+3 -11 days- in Magnitude proposal)	32,000 €
Data processing (1 year)	40,000 €
<b>TOTAL</b>	<b>903,000 €</b>

*Table 2: Cost of microseismic monitoring at Sleipner*

\* This estimate does not include costs associated with installing the tubing, which are also considered in the Work package 4 report.

## 5. Conclusion

In general, the principal advantage of using microseismic monitoring is its continuous nature. In other words, if a cause and effect link is made between the appearance of microseismicity and the increase in pore pressure in the reservoir due to the flow of CO<sub>2</sub>, then, theoretically, a real-time picture is provided of the passage of CO<sub>2</sub> at certain specific points. It is also possible to characterize zones of weakness in the reservoir (or its cover), where pre-existing fractures or joints move in brittle shear and therefore constitute preferential flow axes.

From a practical point of view, microseismicity appears mainly in low-porosity carbonate rocks and when injection pressures are relatively high (several tens of MPa). Given the porosity values at Sleipner, microseismicity is unlikely to appear in the Utsira Formation except in shale lenses or at the top of the formation. This latter case could be the most interesting to monitor as it would reveal the presence of leakage in the caprock. However, it remains to be proven that microseismicity actually does exist.

Clearly, under these conditions, microseismic monitoring is not the preferred tool for monitoring CO<sub>2</sub> injection. However, in terms of drilling observation wells, we recommend:

- choosing the option of installing permanent geophones on the tubing of well 2 for repeated VSP;
- adding a system for continuously recording seismic background noise using these sensors.

With this, it will be possible to detect any microearthquake that is located within about half a kilometre of the well and to attempt to associate it with the shales of the Utsira Formation or those of the overlying Nordland Formation. The additional cost of the continuous recording system and data processing for one year is estimated at approximately 92 000 €.

Even if microseismicity monitoring has not proven to be very suitable at Sleipner, the examples reviewed in chapter 2 show that it could be appropriated to other CO<sub>2</sub> underground storage projects, particularly in low permeability reservoirs. Consequently, we suggest including it in the SACS "Best Practise Manual" for CO<sub>2</sub> storage in saline aquifers.



## 6. References

### REFERENCES FOR SECTION 1: MICROSEISMICITY MONITORING EXAMPLES

#### Underground gas storage

Deflandre, J.P., Laurent, J., Michon, D. and Blondin, E., 1995, *Microseismic surveying and repeated VSPs for monitoring an underground gas storage reservoir using permanent geophones*, First Break, Vol. 13, No.4, 129-138.

#### Oil reservoirs (USA)

Phillips, W.S., T.D. Fairbanks, J.T. Rutledge and D.W. Anderson, 1998a, *Induced Microearthquake Patterns and Oil-Producing Fracture Systems in the Austin Chalk*, Tectonophysics (special issue on induced seismicity), 289, 153-169.

Phillips, W.S., J.T. Rutledge, T.D. Fairbanks, T.L. Gardner, M.E. Miller and B.S. Maher, 1998b, *Reservoir fracture mapping using microearthquakes: Two oilfield case studies*, Soc. Petrol. Eng. (SPE#36651), Reservoir Evaluation & Engineering, 11 p.

Phillips, W.S., Rutledge, J.T., House, L.S. and Fehler, M.C., 2000, *Induced microearthquake patterns in hydrocarbon and geothermal reservoirs*, submitted to *Pure and Applied Geophysics*, March, 2000.

Rutledge, J.T. and Phillips, W.S., 2001, *High-resolution microseismic imaging of a hydraulic fracture, Carthage Cotton Valley gas field, East Texas*, submitted to *Geophysics*, March 2001.

Rutledge, J.T., Phillips, W.S. and B.K. Schuessler, 1998a, *Reservoir Characterization Using Oil-Production-Induced Microseismicity, Clinton County, Kentucky*, Tectonophysics (special issue on induced seismicity), 289, 129-152.

Rutledge, J.T., Phillips, W.S., House, L.S. and Zinno, R.J., 1998b, *Microseismic mapping of a Cotton Valley hydraulic fracture using decimated downhole arrays*, Expanded Abstracts, 338-341, Annual Meeting of the Society of Exploration Geophysicists, New Orleans, Louisiana, September, 338-341.

Withers, R.J. and Rieven, S.A. (1996), *Fracture development during cuttings injection determined by passive seismic monitoring*, SEG 66<sup>th</sup> Ann. Meeting, 106-109.

#### Ekofisk

- Maxwell, S.C., Young, R.P., Bossu, R., Jupe, A. and Dangerfield, J., 1998, *Processing of induced microseismicity recorded in the Ekofisk reservoir*, 68<sup>th</sup> Annual Meeting, Society of Exploration Geophysicist, 904-907.
- Maxwell, S.C., Young, R.P., Bossu, R., Jupe, A. and Dangerfield, J., 1998, *Microseismic logging of the Ekofisk reservoir*, (SPE#47276), Proceedings of EUROCK'98 387-394.

### **Geothermal fields and hydraulic fracturing**

- Eberhart-Phillips, D. and Oppenheimer, D.H., 1984, *Induced seismicity in the Geysers geothermal area, California*, J. of Geophys. Res., 89, 1191-1207.
- Fabriol H. and Munguía, L., (1997), *Seismic Activity at the Cerro Prieto geothermal area (Mexico) from August 1994 to December 1995, and its relationship with tectonics and fluid exploitation*, Geophys. Res. Lett., Vol. 24 (14), pp. 1807-1810.
- Rutledge, J.T., Stark, M.A., Fairbanks, T.D., Anderson, T.D., 2000, *Near-surface microearthquakes at The Geysers geothermal field, California*, submitted to Pure and Applied Geophysics, April, 2000.
- Saaki, S., 1998, *Characteristics of microseismic events induced during hydraulic fracturing experiments at the Hijiori hot dry rock geothermal energy site, Yamagata, Japan*, Tectonophysics (special issue on induced seismicity), 289, 171-188.

### **OTHER REFERENCES**

- Albright, J.N., Rutledge, J., Fairbanks, T.D., Thomson J.C. and Stevenson, M.A. (1998), *Vertical Array for Fracture Mapping in Geothermal Systems*, Transactions, Vol. 22, Geothermal Resources Council Annual Meeting, 20-23 September 1998, San Diego, California, pp. 459-463.
- Bungum, H., Lindholm, C.D., Dahle, A., Woo, G., Nadim, F., Holme, J.K., Gudmestad, O.T., Hagberg, T. and Karthigeyan, K., 2000, *New seismic Zoning Maps for Norway, the North Sea, and the United Kingdom*, Seis. Res. Let. Vol. 71, Num. 6, pp. 687- 697.
- Bungum, H., Alsaker, A., Kvamme, L.B. and Hansen, R.A., 1991, *Seismicity and seismotectonics of Norway and nearby continental shelf areas*, J. of Geoph. Res., Vol. 96, B2, 2249-2265.
- Bungum H. and Dahle, A., 1989, *On the determination of seismic hazards in norwegian continental shelf areas*, in *Earthquakes at North-Atlantic Passive Margins : Neotectonics and Postglacial Rebound*, Gregersen, S. and Basham, P.W., Eds, NATO ASI Series, Series C : Mathematical and Physical Sciences - Vol. 266, pp 665-677

- Bungum, H. and Selnes, P.B. (Eds.), 1988, ELOCS : Earthquake Loading on the Norwegian Continental Shelf, Summary report. Norwegian Geotechnical Institute , NTNF/NORSAR and Principia Mechanica Ltd.
- Burton, P.W. and Marow, P.C., 1989, *Seismic hazard and earthquake source parameters in the North Sea*, in *Earthquakes at North-Atlantic Passive Margins : Neotectonics and Postglacial Rebound*, Gregersen, S. and Basham, P.W., Eds., NATO ASI Series, Series C : Mathematical and Physical Sciences - Vol. 266, pp 601-631.
- Carlsen, M., Mjaaland S. and Nyhavn, F., 2001, *SACS- 2, work package 4. Monitoring well scenarios*, SINTEF, Report 32.1021.00/01/01.
- Coppersmith, K.J. and Youngs R.R., 1989, *Issues regarding earthquake source characterization and seismic hazard analysis within passive margins and stable continental interiors*, in *Earthquakes at North-Atlantic Passive Margins : Neotectonics and Postglacial Rebound*, Gregersen, S. and Basham, P.W., Editors, NATO ASI Series, Series C : Mathematical and Physical Sciences - Vol. 266, pp 601-631.
- Fehler, M.C., House, L.S. and Kaieda, H., 1987, *Determining planes along which earthquakes occur: method and application to earthquakes accompanying hydraulic fracturing*, J. Geophys. Res., 92, 9407-9414.
- Fehler, M.C., Phillips, W.S., House, L.S., Jones, R.H., Aster, R. and Rowe, C.A., 2000, *A method for improving relative earthquakes locations*, Bull. Seism. Soc. Am., 90, 775-780.
- Gölke, M. and Brudy, M., 1996, *Orientation of crustal stresses in the North Sea and Barents Sea inferred from borehole breakouts*, Tectonophysics, 266, 25-32.
- Gölke, M., Clothing, S. and Coblenz D., 1996, *Finite element modelling of stress patterns along Mid-Norwegian continental margin, 62° to 68°N*, Tectonophysics, 266, 33-53.
- Gregersen S. and Basham, P.W., 1989, *Earthquakes at North-Atlantic Passive Margins: Neotectonics and Postglacial Rebound*, NATO ASI Series, Series C: Mathematical and Physical Sciences, Vol. 266, 686 p.
- Grollmund, B., Zoback, M., Wiprut, D.J. and Arnesen, L., 2000, *Stress orientation, pore pressure and the least principal stress in the Norwegian sector of the North Sea* (Accepted for publication in Petroleum Geoscience).
- Herzog, H., Eliasson, B. and Kaarstad, K., 2000, *Capturing Greenhouse Gases*, Scientific America, Vol. 2828, No. 2, 72-79
- Jones, R.H. and Stewart, R.C., 1997, *A method for determining significant structures in a cloud of earthquakes*, J. Geophys. Res., 102, 8245-8254.

- King, G.C.P., Stein, R.S. and Lin, J., 1994, *Static Stress Changes and the Triggering of Earthquakes*, Bull. Seism. Soc. Am., Vol. 84, No. 3, 935-953.
- Liu E., Li, X.Y. and Chadwick, A., 2001, *Multicomponent seismic monitoring of CO<sub>2</sub> gas cloud in the Utsira Sand: A feasibility study*, BGS Commissioned Report C/01/0664.
- Poupinet, G., Ellsworth, W.H. and Fréchet, J., 1984, *Monitoring velocity variations in the crust using earthquakes doublets: An application to the Calaveras Fault, California*, J. Geophys. Res., 89, 5719-5731.
- Ritsema, A.R. and Gürpınar, A., Ed., 1983, *Seismicity and Seismic Risk in the Offshore North Sea Area*, NATO Advanced Study Institutes Series, D. Reidel Publishing Company, 420 p.
- Ritsema, A. R., 1981, *On the assessment of seismic risk in the North Sea Area*, Koninklijk Nederlands Meteorologisch Instituut Report, 19 pp.
- Simpson, D.W., Leith, W.S. and Scholz, C., 1988, *Two types of reservoir induced seismicity*, Bull. Seism. Soc. Am., Vol. 78, No. 6, 2025-2040.
- Srinivasan, C., Arora, S.K. and Benady, S., 1999, *Precursory monitoring of impending rockbursts in Kolar gold mines from microseismic emissions at deeper levels*, Int. J. Rock. Mech. Min. Sci., Vol. 36, No. 7, 941-948.
- Wahlström, R. and Grünthal, G., 2001, *Probabilistic Seismic Hazard Assessment (Horizontal PGA) for Fennoscandia Using the Logic Tree Approach for Regionalization and Nonregionalization Models*, Seis. Res. Let. Vol. 72, Num. 1, pp. 33- 45.
- Wiprut, D., and M.D. Zoback, 2000, *Fault reactivation and fluid flow along a previously dormant normal fault in the Norwegian North Sea*, Geology, Vol. 28, No. 7, 595-598.

## List of Figures

Fig. 1:	Location of the Sleipner hydrocarbon field.....	8
Fig. 2:	Principle of CO <sub>2</sub> sequestering at Sleipner.....	8
Fig. 3:	Interpretation of the comparison between seismic work from 1994 and 1999. The iso-surfaces correspond to a factor 3 increase in reflectivity compared to the original top Utsira reflection. The green surface is top Utsira and the blue surface is base Utsira (SACS2 internal report, 2000). .....	9
Fig. 4:	Germigny-sous-Coulombs gas storage facility. Map of the isobaths of the Wealden reservoir top. Location of well MC7 and extent of the gas bubble in February and November 1991 are shown (from Deflandre et al., 1995). .....	12
Fig. 5:	On-tubing permanent geophones: a) schematic diagram of the three-level string inside well MC7; b) detailed diagram of an on-tubing permanent geophone (op. cit.).....	12
Fig. 6:	Relationship between acoustic activity and variations of gas volumes in relation to injection and withdrawal (over a seven-month period). The survey periods are shown by grey areas. Negative values correspond to gas volumes withdrawn and positive ones to injected volumes. The number of microseismic events recorded per day (one to three) is given in the histogram in the upper part of the Fig. (op. cit.). .....	13
Fig. 7:	2D location of microseismic events. G1, G2 and G3 are sensors (op. cit.) .....	14
Fig. 8:	Map and cross-section views of events located in the Lower Frio during the waste injection experiment. Arrows show cross-section view directions. In cross section views, the thick lines represent the geophones string locations. The gap in the injection well represents the injection interval (from Phillips et al., 2000).....	16
Fig. 9:	Depth view of treatment and monitor wells. Three hydraulic fracture completion stages were conducted in the treatment well 21-10. Geophone stations used in determining the stage 3 microearthquake locations are shown (from Rutledge and Phillips, 2001). .....	18
Fig. 10:	Comparison between variations of bottomhole pressure data with time and induced microseismic event count (op. cit.).....	18
Fig. 11:	Locations of microseismicity during stage 3. Dashed lines in the depth view mark the perforated interval. Some representative error ellipsoid projections are shown (op. cit.). .....	19
Fig. 12:	Same as Fig. 11, after obtaining higher-precision arrival-time data. ....	20
Fig. 13:	Comparison between the depth distribution of microearthquakes and the radioactive proppant tracer log. The dark vertical lines labelled A to F mark the exact stage 3 perforation schedule of the treatment well 21-10 (op.cit.). .....	21
Fig. 14:	Composite focal mechanisms using P-wave first motion for two groupings of all events occurring east of the treatment well (op.cit.). .....	22
Fig. 15:	Different examples of downhole monitoring (source CREATECH Industrie).28	
Fig. 16:	IFP SIMFRAC™ tool.....	29
Fig. 17:	IFP SIMFRAC™ tool installation diagram.....	30
Fig. 18:	Permanent microseismic monitoring probe placed between tubing and casing (source CREATECH Industrie).....	31

Fig. 19: Location of Fenton Hill events within a cube having 400-m sides; (a) locations from the single-event location method, (b) JHD locations, (c) locations from the JHD-collapsing method, (d) locations using relative arrival time picks for the subset of events exhibiting similar waveforms (from Fehler et al., 2000). 34

Fig. 20: Focal mechanism and in situ stress measurement (solid circles) in Western Norway and in the Northern North Sea. Details about events 1 to 6 are given in the text. The lines through the focal sphere projection indicate the direction of P axes (maximum compressive stress). The two parallel NW-SE trending lines across the map are “ridge push” or flow lines computed on the basis of a spreading pole at 52°N, 12.9°E. FZ = fault zone (from Bungum et al., 1991). 38

Fig. 21: Lateral variations of the least principal stress normalised by the vertical stress ( $S_3/S_V$ ) for different depth slices.  $S_3$  is derived from leak-off tests and  $S_V$  comes from the integrated density logs. The Fig. shows that  $S_3/S_V$  is consistently low close to the Norwegian coast and increases towards the west (perpendicular to the coastline). The black lines indicate  $S_{Hmax}$  orientation (from Grollimund et al., 2000). ..... 39

Fig. 22: Earthquake distribution for three different times periods, for Southern Norway and surrounding areas. Different magnitude thresholds are used in each case, but always with symbol size proportional to magnitude. Sleipner is indicated by a star (from Bungum et al., 1991). ..... 56

Fig. 23: Major steps in probabilistic seismic hazard analysis (from Coppersmith and Youngs, 1989) ..... 57

Fig. 24: Seismic zonation for the norwegian continental shelf in term of expected peak ground acceleration (PGA in  $m/s^2$ ) for an exceedance probability of 0.0021/year, i.e. a return period of 475 years. Detailed seismic source zones as used in the hazard estimation are indicated by thin black lines. The thick black line indicates the national sector line. Sleipner field is indicated by a star (from Bungum et al., 2000). ..... 59

## List of tables

Table 1: Comparison between different historical cases of induced microseismicity . 26

Table 2: Cost of microseismic monitoring at Sleipner..... 44

Table 3: Forecast of largest magnitude  $M(T)$ , with uncertainty in brackets, for a range of T-year average return periods..... 58

## **Appendices**



## Appendix 1

### A brief insight into seismic hazard

Seismic hazard is not negligible in the North Sea, firstly because earthquakes of magnitude greater than 5 have been recorded in the area (Fig. 22) and secondly, because operating oil fields represent a significant stake. Seismic hazard has been the subject of various workshops held in the 1980s under the aegis of NATO (Ritsema and Gürpınar, 1983, Gregersen and Basham, 1989). The Norwegian Petroleum Directorate (NPD) has developed a set of earthquake design regulations in 1984, to incorporate this hazard into the design of platforms and all undersea equipment (tubing, wellheads, etc.). A new international standard (ISO) for “Offshore structures for petroleum and gas industries” is being developed, in which a “Northwest European appendix” will be added, elaborated by NPD in partnership with offshore contractors and the Health and Safety Executive (HSE) from UK (Bungum *et al.*, 2000).

In the case of CO<sub>2</sub> storage in the Utsira Formation, there is a new problem: the risk that over time, CO<sub>2</sub> will migrate close to the surface and a sufficiently strong earthquake will occur to create a leak either directly through surface failure or as a result of CO<sub>2</sub> reaching an environment that is in direct contact with the seafloor. This merits consideration, if only to respond to possible criticism about project safety. In the recent study of Bungum *et al.* (*op. cit.*), a new seismic zonation map, based on standard probabilistic hazard evaluation methods and using available regional data, has been proposed for offshore Norway. We recommend that this study be taken into consideration, at a scale adapted to take into account seismic source areas that could affect Sleipner, to evaluate input motion (acceleration and displacement) corresponding to the maximum earthquake at sea bottom and underneath at different depths. It is noteworthy that soil response amplification should also be considered for the evaluation of motion at sea bottom.

Basic elements of a probabilistic study of seismic hazard (Fig. 23) are the following (Coppersmith and Youngs, 1989):

1. Definition of the source zones where the future earthquakes would be localised, either volumes or faults, according to the degree of knowledge;
2. Evaluation of the récurrente relationship for each zone source, describing the frequency of recurrence for earthquakes of various magnitudes until the maximum magnitude. The maximum magnitude that a zone source is able to produce is difficult to define insofar as historical knowledge is limited;
3. Choice of the strong motion attenuation model, which represents the decrease of the energy radiated by an earthquake according to magnitude and distance. Many laws have been calculated starting from the experimental data, for various areas of the

world and various geodynamic contexts;

3. Calculation of curves or maps of ground motion, expressed in the form of peak ground acceleration (PGA), spectral acceleration or ground velocity for an exceedance probability over a given return period. For example, 10 % probability of exceedance in 50 years, or 0.0021 per year exceedance probability, corresponds to a return period of 475 years

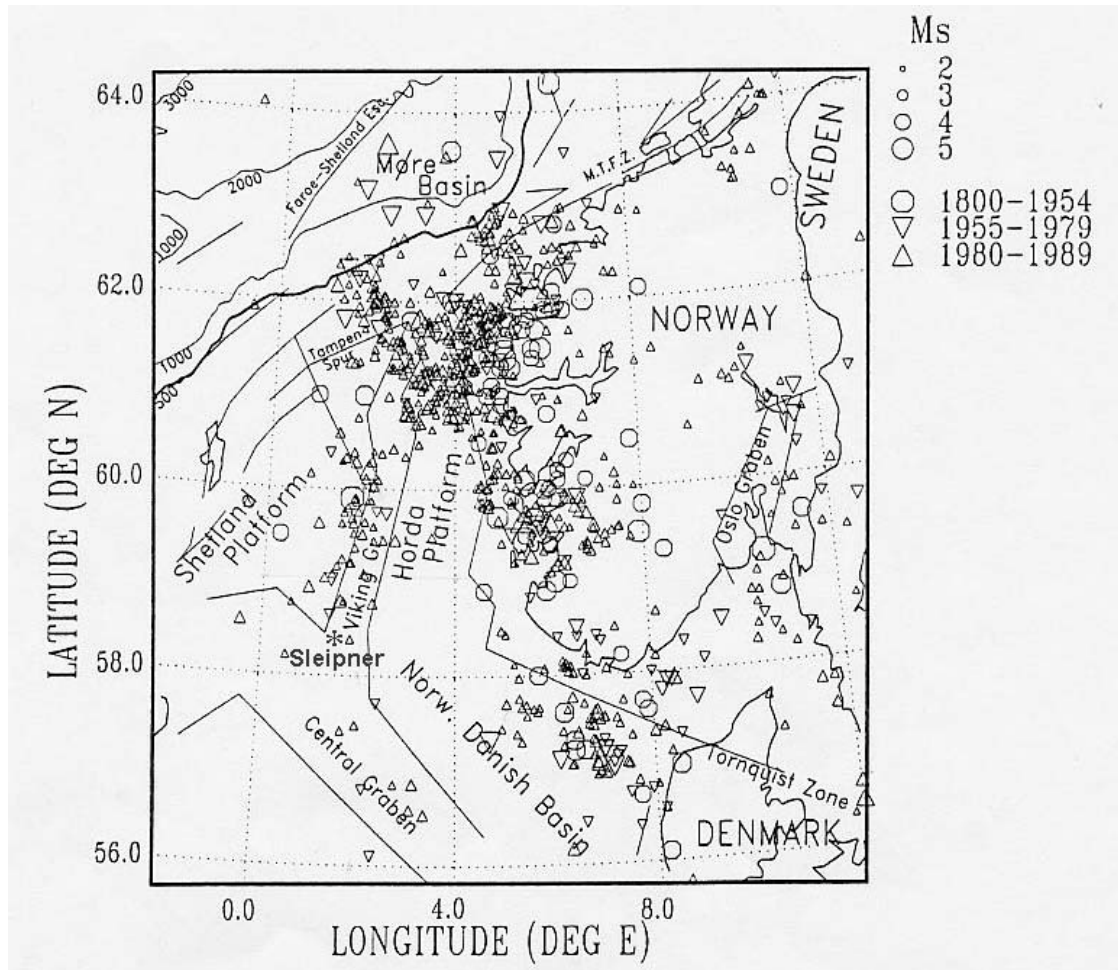


**Fig. 22:** Earthquake distribution for three different times periods, for Southern Norway and surrounding areas. Different magnitude thresholds are used in each case, but always with symbol size proportional to magnitude. Sleipner is indicated by a star (from Bungum et al., 1991).

The probabilistic evaluation of seismic hazard offers the advantage of combining all the possible source zones, with all the earthquakes with various magnitudes and various frequencies of appearance. It also makes it possible to take into account various uncertainties on the input data (mainly the definitions of the source zones and the earthquakes catalogues) and with all the stages of calculation, in order to quantify the error on the final result. The use of logic-trees helps to consider all the possible solutions for the model parameters and, moreover, to weight them by taking into account professional judgement.

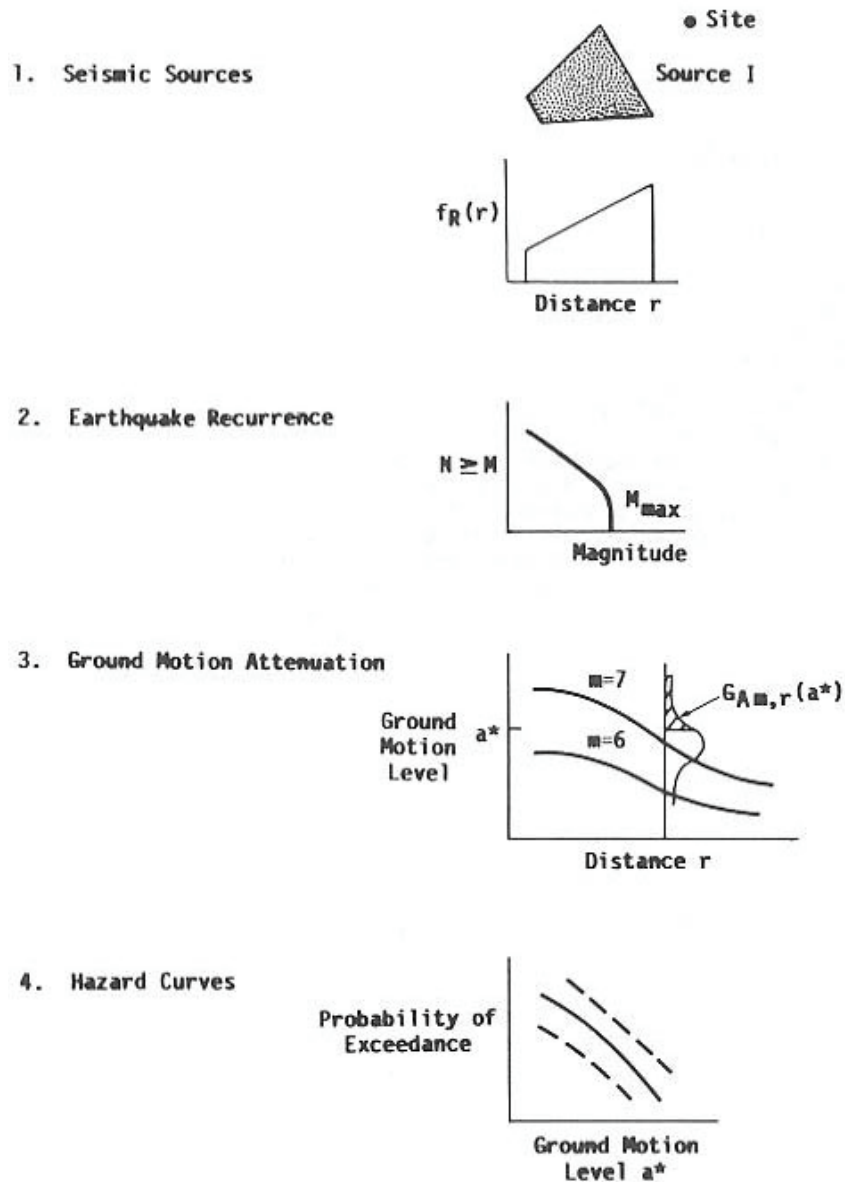


**Fig. 23: Major steps in probabilistic seismic hazard analysis (from Coppersmith and Youngs, 1989)**

Burton and Marrow (1989) calculated for the North Sea (in sector  $57^\circ$ - $64^\circ$  N and  $0^\circ$ - $7^\circ$  S) the probable magnitudes of earthquakes for various return periods (Tab. 3). This evaluation would require to be revised, since it was calculated with catalogues of seismicity until 1979. It shows however that earthquakes with magnitudes circa  $M=6$  can be awaited in the area within the 100 to 200 next years.

T-year	M(T)	T-year	M(T)
5	4.6 (.4)		
10	5.1 (.2)	200	6.3 (.6)
15	5.4 (.2)	500	6.5 (.9)
25	5.6 (.2)	1 000	6.6 (1.1)
50	5.9 (.2)	5 000	6.7 (1.6)
75	6.0 (.3)	7 000	6.7 (1.7)
100	6.1 (.4)	10 000	6.8 (1.8)

**Table 3:** *Forecast of largest magnitude  $M(T)$ , with uncertainty in brackets, for a range of T-year average return periods. Data analysed are two-year extremes in Ritsema's (1981) catalogue for 1900-1979 within 7° longitude (about 770 km) of 57°N, 0° using the Gumbel III distribution. Inversion of probabilities to average return period should be interpreted cautiously, as should extrapolations beyond catalogue duration (from Burton and Marrow, 1989).*

Finally, a map of expected peak ground accélération (PGA), for a return period of 475 years, is presented in the work of Bungum *et al.*, 2000, (Fig. 24). Sleipner is located in the zone where the PGA is close to 0.4 m/s<sup>2</sup>, i.e. less 0.04g. The hazard should not however be minimized, knowing that a facility as that of the storage of CO<sub>2</sub> must be concerned by much longer return periods, of about 1000 to 5000 years. Then, PGA would be higher since that corresponds to earthquakes magnitude closer to M=6.7 than to M=6 (Tab. 3).

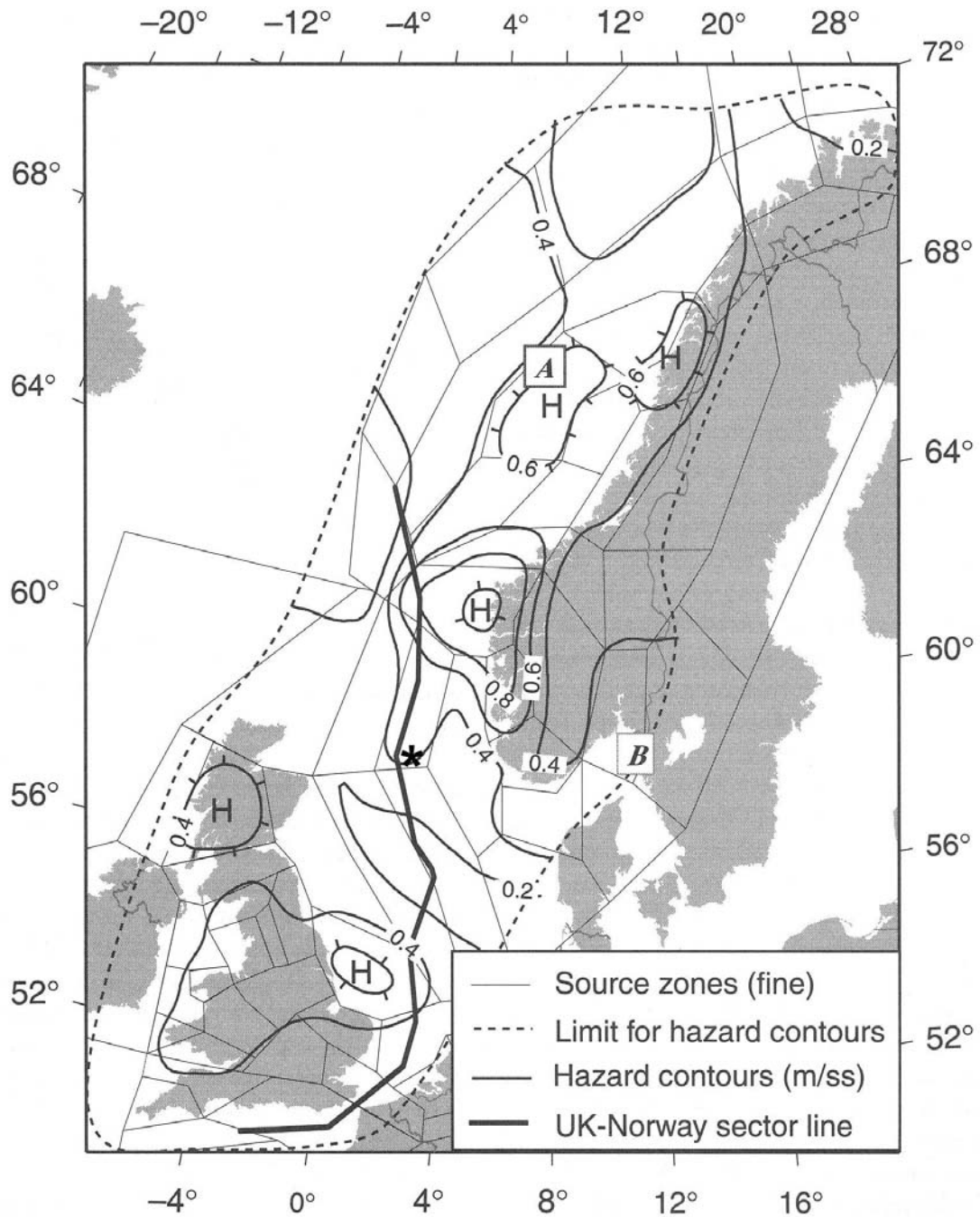
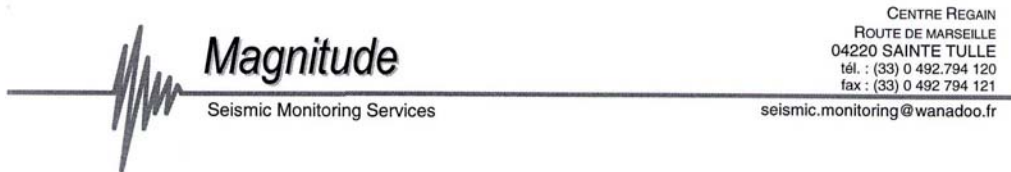


**Fig. 24:** Seismic zonation for the norwegian continental shelf in term of expected peak ground acceleration (PGA in  $m/s^2$ ) for an exceedance probability of 0.0021/year, i.e. a return period of 475 years. Detailed seismic source zones as used in the hazard estimation are indicated by thin black lines. The thick black line indicates the national sector line. Sleipner field is indicated by a star (from Bungum et al., 2000).



## Appendix 2

**Magnitude proposal for follow up of the seismic network and design, setting and periodical update of the automatic monitoring procedures.**



**Subject:** Injection at/below reservoir level

**Requirement:** Proposal to be established with various options from design to permanent management and data analysis.

### Technical proposal

**Site:** XXXXX field – North Sea

**General Objective:** **LONG TERM MONITORING**

- Follow up of the seismic monitoring network.
- Design, setting and periodical update of automatic procedures
- Interpretation of the seismicity recorded

**Type of services:**

- > *Visit on site*
- > *Delivery of monitoring procedure*
- > *Remote assistance*
- > *Data analysis (Standard Micro-Seismic analysis)*
- > *Periodical reporting*
- > *Results presentation/review (correlation with injection)*

**Network:** Geometry of network

The Network is a Mono Well Multi receiver Network (array of Triaxis geophone):

Geometry : cylindrical symmetry – Sub Horizontal axis  
Sensitivity : radial evolution  
Accuracy : *cylindrical symmetry => uncertainty on azimuth & inclination.*  
*distance to the well also controlled by delay between sensors.*

*coupling of each level depends on geology, casing & cement bound => position of geophones greatly depends on well parameters.*

The spacing between geophone is not yet established.

The spacing should be reviewed taking into account the coverage , the sensitivity and the accuracy required.

Basically with 3 levels, Magnitude recommends a solution with a short spacing between level 1 and 2 and a long spacing between level 2 and 3.

**Costs**

<b><u>Step 1</u></b> <b>(alone without other services)</b>	Review of design	<b>Lump Sum</b> <i>One visit (2 days) included</i> <i>Visit from Paris to Paris</i>  <b>100% upon delivery of Report</b>  <b>Travel expenses at cost + 10%</b>	<b>5 000 US\$</b>
<b><u>Step 1+2</u></b>	Monitoring procedure & Monitoring software	<b>Lump Sum</b> <i>One visit (2 days) included</i>  <b>30% upon ordering</b> <b>70% upon delivery of procedures</b>  <b>Travel expenses at cost + 10%</b>	<b>14 000 US\$</b>
<b><u>Step 3</u></b>	Setting of parameters	<b>Visit on site</b> <b>Daily rate</b>  <b>Charged From Paris to Paris</b> <b>100% after the visit</b>  <b>Travel expenses at cost + 10%</b>	<b>1000 US\$/day</b>
<b><u>Step 4</u></b>	Quality Control & Periodical analysis	<b>Lump Sum/year</b> <i>One visit (2 days) included</i>  <b>Payment on a quarterly basis</b> <b>9000 US\$ every quarter</b>  <b>Travel expenses at cost + 10%</b>	<b>36 000 US\$/year</b>
<b><u>Step 5</u></b>	Full analysis & Interpretation	<b>To be defined in step 3</b>	<b>Typically equivalent to step 4</b>

**Check List for INPUT DATA**

*initial review*

1. **General objective / Confidentiality agreement**
2. **Identification of Engineers concerned by the job**
  
3. **General Map (Location of wells)**
4. **General Geological context / Litho / Tectonic features**
  
5. **Formation Velocity**
  - Advanced Sonic Log (P & S Waves) + CBL/Density/GR
  - Crosswell Survey
6. **•Receiver Orientation**
  - Perforations
  - Air Gun Or Other Source•Surveys–Surface Survey (Well-to-well) (3D seismic ?)
  - Deviation Surveys and Well completion design
8. **Type of treatment inducing seismicity**
9. **Parameters available for correlation (type of data and format)**
10. **Scope of work & Procedures**
11. **Geometry of seismic array / Distance from injection points to first seismic sensor**
12. **Type of sensors with respect to frequency expected**
  
13. **Background noise expected (drilling, production...)**
14. **Background natural seismicity or seismicity induced by other causes**
  
15. **Instrument room for surface acquisition system (UPS, telephone line... )**
16. **Data communication from acquisition system to supervisor**
17. **Type of backup system for data**
18. **Data format (Raw data, attributes, map, chronogram...)**

**BRGM**

**SERVICE AMENAGEMENT ET RISQUES NATURELS**

**Unité Mesure, Reconnaissance, Surveillance**

117, avenue de Luminy - BP 167 – 13276 MARSEILLE Cedex 9 - France – Tél. : (33) 04 91 17 74 74